L(6+7): A Unified Lagrangian Across Scales

Cosmology (FRW), Mesoscale UFT, and Vector Photoproduction

Oleg Z.
l67.ai

December 16, 2025

Abstract

We present the L(6+7) framework, a unified variational construction in which cosmological, mesoscale, and microscopic dynamics arise from a single Lagrangian system. The notation (6+7) denotes a decomposition into the standard six-dimensional cosmological sector and an additional seven-dimensional internal state space encoding entropy-driven and statistical degrees of freedom.

In the limit where the internal dynamics are frozen or dynamically suppressed, the theory reduces exactly to the ΛCDM cosmology. Away from this limit, the internal sector generates a structured entropy landscape in which late-time accelerated expansion and dark-matter–like behavior emerge as dynamical regimes, rather than as independent fundamental components.

Using a large numerical ensemble of Friedmann–Robertson–Walker realizations ($\sim 10^5$ trajectories), we identify a compact de Sitter–like attractor basin in parameter space and demonstrate statistically robust correlations between entropy-related indicators and effective matter fractions. These correlations provide a unified statistical interpretation of both dark energy and dark matter within the same underlying dynamics.

Within the L(6+7) framework, the ordering of cosmological histories admits an operational interpretation in terms of an entropic time variable associated with the accessibility of configurations in the extended state space. The same Lagrangian structure consistently induces mesoscale dynamics and controlled corrections to vector photoproduction amplitudes, establishing a direct correspondence between cosmological regimes and microscopic processes.

Taken together, these results indicate that L(6+7) provides a genuinely cross-scale, entropy-structured description in which cosmology, effective field theory, and local particle phenomena emerge from a single unified dynamical principle.[1]

Contents

1 Introduction

1.1 Variational starting point

We consider a dynamical system defined by a single action functional

$$S = \int dt\, L, \tag{1.1}$$

where the Lagrangian L is assumed to govern all relevant regimes of the theory. The central hypothesis of the present work is that cosmological dynamics, mesoscale effective behavior, and microscopic processes correspond to different reductions of the same underlying Lagrangian structure.

The configuration space is taken to be

$$\mathcal{Q} = \{a(t), X_A(t)\}, \qquad A = 1, \ldots, 7, \tag{1.2}$$

where $a(t)$ is the cosmological scale factor and X_A denote internal variables associated with entropy and probabilistic structure.

1.2 Reduction principle

The reduction principle is defined as follows. Let

$$L_{6+7}(a, \dot{a}; X_A, \dot{X}_A) \tag{1.3}$$

be the full Lagrangian. Then:

- The *cosmological reduction* is obtained by integrating out or freezing the internal variables:

$$X_A = \text{const}, \qquad \dot{X}_A = 0. \tag{1.4}$$

- The *effective-field reduction* corresponds to coarse-graining over subsets of $\{X_A\}$.
- The *microscopic reduction* probes fluctuations around localized trajectories in the full configuration space.

All reductions preserve the variational origin of the equations of motion.

1.3 Recovery of standard cosmology

Under the freezing condition,

$$\mathcal{L}_7(X_A, \dot{X}_A; a) \longrightarrow -\rho_\Lambda, \tag{1.5}$$

the action reduces to

$$S \to \int dt \left[-\frac{3}{8\pi G} a\dot{a}^2 - a^3 \rho_{\mathrm{m}}(a) - a^3 \rho_\Lambda \right], \tag{1.6}$$

which yields the standard Friedmann equation

$$\left(\frac{\dot{a}}{a}\right)^2 = \frac{8\pi G}{3} \left(\rho_{\mathrm{m}} + \rho_\Lambda\right). \tag{1.7}$$

Thus, ΛCDM is recovered as a strict limiting case of the theory, consistent with the standard Friedmann–Lemaître–Robertson–Walker framework [1, 2, 3, 4].

1.4 Emergent interpretation of dark sectors

When the internal variables are dynamical, the Hamiltonian constraint takes the general form

$$H = -\frac{4\pi G}{3a} p_a^2 + a^3 \rho_{\rm m}(a) + H_7(X_A, p_A; a) = 0. \tag{1.8}$$

This can be rewritten as

$$\left(\frac{\dot{a}}{a}\right)^2 = \frac{8\pi G}{3} \left(\rho_{\rm m} + \rho_7^{\rm eff}(a)\right), \tag{1.9}$$

where

$$\rho_7^{\rm eff}(a) \equiv \frac{H_7}{a^3}. \tag{1.10}$$

Dark-energy–like and dark-matter–like behaviors correspond to different functional dependencies of $\rho_7^{\rm eff}(a)$, determined by the entropy structure of the internal sector rather than by independent physical fluids.

1.5 Cross-scale meaning

Because the same Lagrangian generates all equations of motion, the reduction from cosmology to mesoscale and microscopic physics preserves functional relations between observables. In particular, the same parameters controlling $\rho_7^{\rm eff}(a)$ also appear in reduced effective-field equations and in corrections to microscopic amplitudes.

This establishes the framework for a genuine cross-scale correspondence explored in subsequent sections.

2 The L(6+7) Lagrangian

2.1 Configuration space and degrees of freedom

The theory is formulated as a variational system on an extended configuration space

$$\mathcal{Q} = \{a(t), X_A(t)\}, \qquad A = 1, \ldots, 7, \tag{2.1}$$

where $a(t)$ denotes the cosmological scale factor and $X_A(t)$ are internal degrees of freedom associated with entropy production, coarse-graining, and probabilistic branching of histories.

The variables X_A do not correspond to additional spacetime dimensions. Instead, they parametrize an internal state space whose geometry and dynamics control the statistical structure of cosmological evolution.

The tangent bundle is therefore

$$T\mathcal{Q} = \{a, \dot{a}; X_A, \dot{X}_A\}, \tag{2.2}$$

and all equations of motion follow from a single action principle defined on $T\mathcal{Q}$.

2.2 Definition of the unified Lagrangian

The unified Lagrangian is defined as

$$\boxed{L_{6+7} = -\frac{3}{8\pi G}\, a\dot{a}^2 - a^3 \rho_{\rm std}(a) + a^3 \mathcal{L}_7(X_A, \dot{X}_A; a)} \tag{2.3}$$

The first term represents the Einstein–Hilbert action reduced to a flat FRW minisuperspace. The second term encodes standard matter and radiation components, while the third term describes the dynamics of the seven-dimensional internal sector.

The standard energy density is given by

$$\rho_{\rm std}(a) = \rho_{\rm m,0} a^{-3} + \rho_{\rm r,0} a^{-4}, \tag{2.4}$$

ensuring consistency with conventional cosmology in the appropriate limit.

2.3 Internal sector structure

The internal-sector Lagrangian is taken in the general nonlinear sigma-model form

$$\mathcal{L}_7 = \frac{1}{2} G_{AB}(X)\, \dot{X}^A \dot{X}^B - V(X; a), \tag{2.5}$$

where $G_{AB}(X)$ is a positive-definite metric on the internal manifold $\mathcal{M}_7$, and $V(X; a)$ is a scale-dependent potential.

The explicit dependence of V on the scale factor a introduces a coupling between cosmological expansion and internal entropy dynamics. This coupling is the key mechanism by which effective dark-energy– and dark-matter–like behavior emerges without introducing additional fundamental substances.

2.4 Canonical momenta and phase space

The canonical momenta associated with the variables (a, X_A) are

$$p_a = \frac{\partial L}{\partial \dot{a}} = -\frac{3}{4\pi G}\, a\dot{a}, \tag{2.6}$$

$$p_A = \frac{\partial L}{\partial \dot{X}^A} = a^3 G_{AB}(X)\, \dot{X}^B. \tag{2.7}$$

These relations can be inverted to express velocities in terms of momenta:

$$\dot{a} = -\frac{4\pi G}{3a}\, p_a, \tag{2.8}$$

$$\dot{X}^A = \frac{1}{a^3} G^{AB}(X)\, p_B. \tag{2.9}$$

The appearance of the factor a^3 in the internal-sector momenta indicates that cosmological expansion directly rescales the effective inertia of the internal degrees of freedom.

2.5 Hamiltonian formulation

The Hamiltonian is obtained via the Legendre transform

$$H = p_a \dot{a} + p_A \dot{X}^A - L. \tag{2.10}$$

Substituting the explicit expressions yields

$$\boxed{H = -\frac{4\pi G}{3a} p_a^2 + a^3 \rho_{\rm std}(a) + H_7(X_A, p_A; a)} \tag{2.11}$$

with the internal-sector Hamiltonian

$$H_7 = \frac{1}{2a^3} G^{AB}(X)\, p_A p_B + a^3 V(X; a). \tag{2.12}$$

The Hamiltonian separates naturally into a gravitational part, a standard matter contribution, and an internal-sector contribution whose relative weight depends explicitly on the cosmological scale.

2.6 Hamiltonian constraint and cosmological dynamics

Time-reparameterization invariance of the action implies the Hamiltonian constraint

$$\boxed{H = 0}. \tag{2.13}$$

Explicitly, this constraint reads

$$-\frac{4\pi G}{3a} p_a^2 + a^3 \rho_{\text{std}}(a) + \frac{1}{2a^3} G^{AB} p_A p_B + a^3 V(X; a) = 0. \tag{2.14}$$

Using the relation between p_a and $\dot{a}$, the constraint can be rewritten as a generalized Friedmann equation:

$$\left(\frac{\dot{a}}{a}\right)^2 = \frac{8\pi G}{3} \left[\rho_{\text{std}}(a) + \rho_7^{\text{eff}}(a)\right], \tag{2.15}$$

where the effective internal energy density is defined as

$$\boxed{\rho_7^{\text{eff}}(a) = \frac{1}{2a^6} G^{AB} p_A p_B + V(X; a).} \tag{2.16}$$

This expression shows explicitly that all deviations from standard cosmology are encoded in the internal-sector Hamiltonian.

2.7 Equations of motion for the internal sector

The equations of motion for the internal variables follow from Hamilton's equations:

$$\dot{X}^A = \frac{\partial H}{\partial p_A}, \qquad \dot{p}_A = -\frac{\partial H}{\partial X^A}. \tag{2.17}$$

In Lagrangian form, they read

$$\ddot{X}^A + 3\frac{\dot{a}}{a}\dot{X}^A + \Gamma^A_{BC}(X)\,\dot{X}^B\dot{X}^C + G^{AB}\partial_B V(X; a) = 0, \tag{2.18}$$

where Γ^A_{BC} are the Christoffel symbols of the internal metric G_{AB}.

The term $3(\dot{a}/a)\dot{X}^A$ acts as a cosmological friction, linking entropy dynamics directly to expansion.

2.8 Reduction limits and physical regimes

Frozen internal sector. If

$$\dot{X}^A = 0, \qquad V(X; a) = \rho_\Lambda, \tag{2.19}$$

then

$$\rho_7^{\text{eff}} = \rho_\Lambda, \tag{2.20}$$

and the standard ΛCDM cosmology is recovered exactly.

Dynamical internal sector. When the internal variables evolve dynamically, the kinetic term contributes

$$\rho_{7,\text{kin}}^{\text{eff}} \propto a^{-6}, \tag{2.21}$$

corresponding to stiff or matter-like effective behavior, depending on the statistical structure of trajectories in $\mathcal{M}_7$.

2.9 Interpretation

The L(6+7) Lagrangian defines a closed, self-consistent variational system in which all effective cosmological components arise from a single internal-sector Hamiltonian. No additional fundamental degrees of freedom are required, and all regime transitions are governed by the entropy structure of the extended state space.

3 Gravity as a Scale Operator

3.1 Operational definition

In the L(6+7) framework, gravity is treated in the standard geometric sense on the FRW minisuperspace, yet it also acquires an operational meaning as a *scale operator* acting on the statistical (entropic) structure of the internal sector. This interpretation is not an additional postulate: it follows from the explicit scale-factor dependence in the Lagrangian weight a^3 and in the internal potential $V(X;a)$.

We begin from the unified action

$$S = \int dt\, L_{6+7} = \int dt \left[-\frac{3}{8\pi G}\, a\dot{a}^2 - a^3 \rho_{\rm std}(a) + a^3 \left(\frac{1}{2} G_{AB}(X) \dot{X}^A \dot{X}^B - V(X;a) \right) \right]. \tag{3.1}$$

The Hamiltonian constraint implies

$$\left(\frac{\dot{a}}{a}\right)^2 = \frac{8\pi G}{3} \left(\rho_{\rm std}(a) + \rho_7^{\rm eff}(a) \right), \qquad \rho_7^{\rm eff}(a) = \frac{1}{2} G_{AB} \dot{X}^A \dot{X}^B + V(X;a), \tag{3.2}$$

which makes the Hubble rate a direct probe of the internal-sector effective energy.

3.2 Scale-flow generator and logarithmic time

To express the "scale-operator" meaning precisely, we introduce the logarithmic scale variable

$$N \equiv \ln a, \qquad \frac{d}{dt} = H \frac{d}{dN}, \qquad H \equiv \frac{\dot{a}}{a}. \tag{3.3}$$

Any scale-dependent quantity $Q(a)$ admits a scale-flow derivative

$$\mathcal{D}_a Q \;\equiv\; \frac{dQ}{dN} \;=\; a \frac{dQ}{da}. \tag{3.4}$$

In this language, gravity acts as an operator generating flow in N via H, because the evolution operator is

$$\frac{d}{dt} = H\, \mathcal{D}_a. \tag{3.5}$$

Thus, in the coupled system, gravity does not only curve spacetime; it determines the rate at which the system is transported along the scale direction in the extended state space.

3.3 Internal-sector energy balance under expansion

Define internal-sector effective density and pressure as

$$\rho_7 \equiv \frac{1}{2} G_{AB} \dot{X}^A \dot{X}^B + V(X;a), \qquad p_7 \equiv \frac{1}{2} G_{AB} \dot{X}^A \dot{X}^B - V(X;a), \qquad w_7 \equiv \frac{p_7}{\rho_7}. \tag{3.6}$$

Using the internal equations of motion

$$\ddot{X}^A + 3H\dot{X}^A + \Gamma^A_{BC} \dot{X}^B \dot{X}^C + G^{AB} \partial_B V(X;a) = 0, \tag{3.7}$$

one obtains the energy-balance identity

$$\dot{\rho}_7 + 3H(\rho_7 + p_7) = \frac{\partial V(X;a)}{\partial a}\,\dot{a} = H\,\frac{\partial V(X;a)}{\partial N}. \tag{3.8}$$

Equivalently, in N-form,

$$\boxed{\frac{d\rho_7}{dN} + 3(\rho_7 + p_7) = \frac{\partial V}{\partial N}.} \tag{3.9}$$

This is the key relation: the scale dependence of $V(X;a)$ injects or extracts effective energy into/from the internal sector as the universe expands. In other words, gravity (through $a(t)$ and H) acts as a driver of the internal-sector energy flow.

3.4 Entropy functional and scale operator

We now formalize the entropic structure by introducing an entropy functional Θ on the internal manifold. A minimal operational definition is

$$\Theta \equiv \log \mu(\mathcal{A}), \tag{3.10}$$

where $\mu(\mathcal{A})$ is the measure (volume) of an accessible subset $\mathcal{A} \subset \mathcal{M}_7$.

If we use the metric measure on $\mathcal{M}_7$,

$$d\mu = \sqrt{g_7(X)}\, d^7X, \qquad g_7 \equiv \det(G_{AB}), \tag{3.11}$$

then the entropy of accessibility can be represented as

$$\Theta(a) = \log\left[\int_{\mathcal{M}_7} d^7X\,\sqrt{g_7(X)}\;W(X;a)\right], \tag{3.12}$$

where $W(X;a)$ is a nonnegative weight encoding which configurations are accessible/selected at scale a.

A canonical thermodynamic-like choice is

$$W(X;a) = \exp(-\beta(a)\,\mathcal{H}_7(X;a))\,, \qquad \mathcal{H}_7(X;a) \equiv \frac{1}{2}G^{AB}p_A p_B + a^6 V(X;a), \tag{3.13}$$

leading to a partition-function form

$$Z(a) = \int d^7X\,\sqrt{g_7}\,e^{-\beta(a)\mathcal{H}_7(X;a)}, \qquad \Theta(a) = \log Z(a). \tag{3.14}$$

The *scale operator* acting on entropy is then

$$\boxed{\mathcal{D}_a\Theta \equiv \frac{d\Theta}{dN} = \frac{1}{Z}\frac{dZ}{dN}.} \tag{3.15}$$

Computing the derivative yields

$$\frac{d\Theta}{dN} = -\left\langle \frac{d\beta}{dN}\,\mathcal{H}_7\right\rangle - \left\langle \beta\,\frac{\partial \mathcal{H}_7}{\partial N}\right\rangle + \frac{1}{2}\left\langle \frac{d}{dN}\log g_7\right\rangle, \tag{3.16}$$

where $\langle\cdot\rangle$ denotes averaging with respect to the weight $W(X;a)/Z(a)$.

This explicitly shows that the evolution of scale a generates a flow in entropy through three channels:

$$\text{(i) } \beta(a)\text{-flow}, \qquad \text{(ii) explicit } \partial_N\mathcal{H}_7 \text{ via } V(X;a), \qquad \text{(iii) metric/volume flow of } g_7(X). \tag{3.17}$$

3.5 Regimes as fixed points of the scale flow

A regime corresponds to a stable scaling behavior of the effective internal density $\rho_7(a)$. Define the logarithmic slope

$$\kappa_7(a) \equiv -\frac{d\ln\rho_7}{d\ln a} = -\frac{d\ln\rho_7}{dN}. \tag{3.18}$$

Using the balance equation, if $\partial_N V \approx 0$ (or averages to a constant), we have approximately

$$\frac{d\rho_7}{dN} \approx -3(\rho_7 + p_7) = -3\rho_7(1 + w_7), \tag{3.19}$$

so that

$$\boxed{\kappa_7 \approx 3(1 + w_7).} \tag{3.20}$$

Hence:

$$w_7 \approx -1 \;\Rightarrow\; \kappa_7 \approx 0 \quad \text{(DE-like)}, \tag{3.21}$$

$$w_7 \approx 0 \;\Rightarrow\; \kappa_7 \approx 3 \quad \text{(matter-like)}, \tag{3.22}$$

$$w_7 \approx 1 \;\Rightarrow\; \kappa_7 \approx 6 \quad \text{(stiff-like)}. \tag{3.23}$$

The DE-like basin corresponds to a dynamical fixed point where ρ_7 becomes approximately constant in N and dominates late-time expansion:

$$\frac{d\rho_7}{dN} \approx 0, \qquad w_7 \approx -1. \tag{3.24}$$

More generally, scale dependence of V modifies the fixed-point condition:

$$\boxed{\frac{d\rho_7}{dN} = -3\rho_7(1 + w_7) + \frac{\partial V}{\partial N}.} \tag{3.25}$$

Thus the internal-sector potential is the control knob for the scale-flow structure, and gravity provides the evolution parameter through $N = \ln a$.

3.6 Summary: meaning of "gravity as a scale operator"

The scale-operator statement is summarized by the chain

$$a(t) \;\Rightarrow\; N = \ln a \;\Rightarrow\; \mathcal{D}_a = \frac{d}{dN} \;\Rightarrow\; \text{flow of } \rho_7,\; w_7,\; \Theta, \tag{3.26}$$

together with the identities

$$\frac{d}{dt} = H\,\mathcal{D}_a, \qquad \frac{d\rho_7}{dN} + 3(\rho_7 + p_7) = \frac{\partial V}{\partial N}, \qquad \mathcal{D}_a\Theta = \frac{1}{Z}\frac{dZ}{dN}. \tag{3.27}$$

Therefore, within L(6+7), gravity acts as an operator that transports the system along the scale direction and thereby reshapes the entropic accessibility and effective energy composition of the universe, producing distinct stable regimes (DE-like, DM-like, stiff-like) as dynamical outcomes of the same unified action.

4 FRW Dynamics in the L(6+7) Framework

4.1 FRW minisuperspace equations

We consider a spatially flat Friedmann–Robertson–Walker spacetime with line element

$$ds^2 = -dt^2 + a^2(t)\,d\vec{x}^2, \tag{4.1}$$

fully characterized by the scale factor $a(t)$.

The dynamics follow from the Hamiltonian constraint of the L(6+7) system,

$$H_{\text{tot}} = -\frac{4\pi G}{3a} p_a^2 + a^3 \rho_{\text{std}}(a) + a^3 \rho_7(a) = 0, \tag{4.2}$$

which yields the generalized Friedmann equation

$$\boxed{H^2 \equiv \left(\frac{\dot{a}}{a}\right)^2 = \frac{8\pi G}{3} \left(\rho_{\text{std}}(a) + \rho_7(a)\right).} \tag{4.3}$$

Here $\rho_{\text{std}} = \rho_m + \rho_r$ denotes the standard matter and radiation densities, while ρ_7 is the effective internal-sector energy density defined in Section 0.2. In the limit $\rho_7 \to \rho_\Lambda = \text{const}$, the above equation reduces to the standard Friedmann equation of ΛCDM cosmology, consistent with classical treatments of FRW dynamics [5].

4.2 Acceleration equation

Variation of the action with respect to $a(t)$ yields the acceleration equation

$$\frac{\ddot{a}}{a} = -\frac{4\pi G}{3} \left[(\rho_{\text{std}} + 3p_{\text{std}}) + (\rho_7 + 3p_7)\right], \tag{4.4}$$

where

$$p_{\text{std}} = p_m + p_r = \frac{1}{3}\rho_r, \tag{4.5}$$

and p_7 is the effective pressure of the internal sector,

$$p_7 = \frac{1}{2} G_{AB} \dot{X}^A \dot{X}^B - V(X; a). \tag{4.6}$$

Cosmic acceleration occurs whenever

$$\rho_7 + 3p_7 < -(\rho_{\text{std}} + 3p_{\text{std}}). \tag{4.7}$$

4.3 Continuity equations

The standard components satisfy the usual continuity equations,

$$\dot{\rho}_m + 3H\rho_m = 0, \qquad \dot{\rho}_r + 4H\rho_r = 0. \tag{4.8}$$

The internal sector obeys the modified continuity equation derived in Section 0.3,

$$\boxed{\dot{\rho}_7 + 3H(\rho_7 + p_7) = \dot{a}\,\frac{\partial V}{\partial a}.} \tag{4.9}$$

In logarithmic scale form ($N = \ln a$),

$$\boxed{\frac{d\rho_7}{dN} = -3(\rho_7 + p_7) + \frac{\partial V}{\partial N}.} \tag{4.10}$$

This equation governs the deviation from standard FRW scaling.

4.4 Effective density parameters

Define the dimensionless density parameters

$$\Omega_i \equiv \frac{8\pi G}{3H^2}\rho_i, \qquad i \in \{m, r, 7\}. \tag{4.11}$$

The Friedmann equation implies the closure condition

$$\boxed{\Omega_m + \Omega_r + \Omega_7 = 1.} \tag{4.12}$$

The internal-sector contribution therefore directly competes with standard matter and radiation in determining the expansion history.

4.5 Effective equation of state

Define the total effective equation-of-state parameter

$$w_{\text{eff}} \equiv \frac{p_{\text{std}} + p_7}{\rho_{\text{std}} + \rho_7}. \tag{4.13}$$

The acceleration equation can then be written as

$$\boxed{\frac{\ddot{a}}{a} = -\frac{1}{2}H^2(1 + 3w_{\text{eff}}).} \tag{4.14}$$

Late-time acceleration corresponds to

$$w_{\text{eff}} < -\frac{1}{3}. \tag{4.15}$$

In the limit $\rho_7 \gg \rho_{\text{std}}$,

$$w_{\text{eff}} \simeq w_7. \tag{4.16}$$

4.6 Deceleration and jerk parameters

To characterize departures from standard expansion, we introduce the cosmographic parameters

$$q \equiv -\frac{\ddot{a}}{aH^2}, \qquad j \equiv \frac{\dddot{a}}{aH^3}. \tag{4.17}$$

Using the effective equation of state,

$$\boxed{q = \frac{1}{2}(1 + 3w_{\text{eff}}).} \tag{4.18}$$

The jerk parameter is obtained by differentiating H,

$$j = 1 + \frac{9}{2}w_{\text{eff}}(1 + w_{\text{eff}}) - \frac{3}{2}\frac{dw_{\text{eff}}}{dN}. \tag{4.19}$$

For ΛCDM, $w_{\text{eff}} = -1$ and $j = 1$, while deviations from unity signal nontrivial internal-sector dynamics.

4.7 Scaling solutions and regimes

Assume a scaling solution of the form

$$\rho_7 \propto a^{-\kappa_7}. \tag{4.20}$$

Then

$$\kappa_7 = -\frac{d\ln\rho_7}{d\ln a}. \tag{4.21}$$

Using the continuity equation,

$$\boxed{\kappa_7 = 3(1 + w_7) - \frac{1}{\rho_7}\frac{\partial V}{\partial N}.} \tag{4.22}$$

Special regimes are classified by κ_7:

$$\kappa_7 \simeq 0 \;\Rightarrow\; \rho_7 \approx \text{const} \quad \text{(DE-like)}, \tag{4.23}$$

$$\kappa_7 \simeq 3 \;\Rightarrow\; \rho_7 \propto a^{-3} \quad \text{(DM-like)}, \tag{4.24}$$

$$\kappa_7 \simeq 6 \;\Rightarrow\; \rho_7 \propto a^{-6} \quad \text{(stiff-like)}. \tag{4.25}$$

These regimes arise dynamically from the same underlying equations.

4.8 Summary of FRW dynamics

The FRW dynamics in the L(6+7) framework are fully governed by the coupled system

$$H^2 = \frac{8\pi G}{3}(\rho_{\rm std} + \rho_7), \tag{4.26}$$

$$\frac{d\rho_7}{dN} = -3(\rho_7 + p_7) + \frac{\partial V}{\partial N}, \tag{4.27}$$

$$p_7 = \frac{1}{2}G_{AB}\dot{X}^A\dot{X}^B - V(X;a). \tag{4.28}$$

All cosmological observables—expansion rate, acceleration, and regime classification—are therefore determined by the internal-sector dynamics encoded in the L(6+7) Lagrangian.

5 Entropy Landscape and Regime Structure

5.1 Definition of the entropy landscape

The dynamical regimes of the L(6+7) system are controlled by the entropy structure of the internal sector. We formalize this structure by introducing an entropy functional defined on the internal configuration manifold $\mathcal{M}_7$.

Let $X^A \in \mathcal{M}_7$ with metric $G_{AB}(X)$ and volume element

$$d\mu_7 = \sqrt{g_7(X)}\, d^7X, \qquad g_7 \equiv \det(G_{AB}). \tag{5.1}$$

We define the entropy landscape as

$$\boxed{\Theta(a) = \log Z(a), \qquad Z(a) \equiv \int_{\mathcal{M}_7} d\mu_7\, W(X;a),} \tag{5.2}$$

where $W(X;a)$ is a nonnegative weight function encoding the statistical accessibility of internal configurations at scale a.

5.2 Canonical statistical weight

A natural and operationally well-defined choice of weight is

$$W(X;a) = \exp[-\beta(a)\,\mathcal{H}_7(X;a)]\,, \tag{5.3}$$

with the internal Hamiltonian density

$$\mathcal{H}_7(X;a) = \frac{1}{2}G^{AB}(X)\,p_A p_B + a^6 V(X;a). \tag{5.4}$$

The parameter $\beta(a)$ plays the role of an effective inverse temperature associated with coarse-graining at scale a.

5.3 Entropy gradients and scale flow

The evolution of entropy with scale is generated by the scale-flow operator $\mathcal{D}_a = d/d\ln a$. Applying this operator yields

$$\mathcal{D}_a\Theta = \frac{1}{Z}\mathcal{D}_a Z. \tag{5.5}$$

Explicitly,

$$\boxed{\mathcal{D}_a\Theta = -\left\langle \mathcal{D}_a(\beta\mathcal{H}_7)\right\rangle + \frac{1}{2}\left\langle \mathcal{D}_a \ln g_7\right\rangle,} \tag{5.6}$$

where angular brackets denote averaging with respect to the normalized weight W/Z.

This equation identifies three independent contributions to entropy flow:

$$\mathcal{D}_a\Theta = -\left\langle \frac{d\beta}{d\ln a}\,\mathcal{H}_7\right\rangle - \left\langle \beta\,\frac{\partial\mathcal{H}_7}{\partial\ln a}\right\rangle + \frac{1}{2}\left\langle \frac{d\ln g_7}{d\ln a}\right\rangle. \tag{5.7}$$

5.4 Entropy force and effective dynamics

Define the entropy gradient in the internal space as

$$\Xi_A \equiv \partial_A \Theta. \tag{5.8}$$

This gradient induces an effective entropic force on trajectories in $\mathcal{M}_7$, modifying their statistical weight. The contribution of entropy gradients to the effective energy density is encoded through the scale derivative of Θ:

$$\boxed{\frac{d\rho_7}{d\ln a} = -3(\rho_7 + p_7) + \frac{\partial V}{\partial \ln a} = \mathcal{F}_\Theta(a),} \tag{5.9}$$

where $\mathcal{F}_\Theta$ represents entropy-driven energy flow.

The use of entropy as an effective organizing principle for dynamical regimes is consistent with earlier approaches to gravitational and statistical coarse-graining [6, 7].

5.5 Regime classification via entropy slopes

Define the entropy slope

$$S(a) \equiv \mathcal{D}_a \Theta = \frac{d\Theta}{d\ln a}. \tag{5.10}$$

We further define the regime indicator

$$\kappa_7(a) \equiv -\frac{d\ln \rho_7}{d\ln a}. \tag{5.11}$$

Combining the continuity equation with entropy flow yields

$$\boxed{\kappa_7 = 3(1 + w_7) - \frac{1}{\rho_7}\frac{\partial V}{\partial \ln a} = \kappa_7(S).} \tag{5.12}$$

Thus, cosmological regimes correspond to characteristic entropy slopes.

5.6 Fixed points and attractors

A dynamical regime corresponds to a fixed point of the entropy flow,

$$\mathcal{D}_a \Theta = S_* = \text{const}. \tag{5.13}$$

At a fixed point,

$$\mathcal{D}_a \rho_7 = 0, \qquad \Rightarrow \qquad 3(1 + w_7)\rho_7 = \frac{\partial V}{\partial \ln a}. \tag{5.14}$$

Special cases include:

$$S_* \approx 0 \;\Rightarrow\; \rho_7 \approx \text{const} \quad \text{(DE-like attractor)}, \tag{5.15}$$

$$S_* \approx \text{const} > 0 \;\Rightarrow\; \rho_7 \propto a^{-3} \quad \text{(DM-like regime)}, \tag{5.16}$$

$$S_* \gg 1 \;\Rightarrow\; \rho_7 \propto a^{-6} \quad \text{(stiff regime)}. \tag{5.17}$$

5.7 Entropy landscape geometry

The entropy landscape induces an effective geometry on parameter space. The Hessian matrix

$$H^\Theta_{AB} \equiv \nabla_A \nabla_B \Theta \tag{5.18}$$

controls stability properties of trajectories.

Stability requires

$$\lambda_{\min}(H^\Theta_{AB}) > 0, \tag{5.19}$$

while saddle points correspond to regime transitions.

5.8 Projection to observable space

In practical numerical implementations, the entropy landscape is projected onto low-dimensional parameter subspaces $\{\lambda_i\}$:

$$\Theta(\lambda_i) = \log\left[\int d^7X \sqrt{g_7}\, W(X;\lambda_i)\right]. \tag{5.20}$$

Observable regime maps correspond to level sets

$$\Theta(\lambda_i) = \text{const}, \tag{5.21}$$

which are visualized in the numerical analysis.

5.9 Summary

The entropy landscape $\Theta(a, X)$ provides a unifying control structure for all dynamical regimes of the L(6+7) framework. Fixed points of entropy flow correspond to stable cosmological regimes, while gradients and Hessians determine transitions and stability. This structure directly underlies the numerical regime maps and phase diagrams presented in subsequent sections.

6 Mesoscale Unified Field Theory

6.1 Mesoscale limit and averaging

The mesoscale regime corresponds to a controlled reduction of the full L(6+7) dynamics in which fast microscopic fluctuations are averaged, while slow collective modes remain dynamical. Let $\mathcal{O}(X_A)$ be an observable on the internal manifold. We define mesoscale averaging by

$$\langle \mathcal{O}\rangle_{\text{ms}}(a) \equiv \frac{1}{Z(a)} \int_{\mathcal{M}_7} d^7X \sqrt{g_7(X)}\, \mathcal{O}(X)\, W(X;a), \tag{6.1}$$

with partition function

$$Z(a) = \int_{\mathcal{M}_7} d^7X \sqrt{g_7(X)}\, W(X;a), \qquad W(X;a) = e^{-\beta(a)\mathcal{H}_7(X;a)}. \tag{6.2}$$

This averaging defines effective mesoscale fields as entropy-weighted collective variables.

6.2 Effective mesoscale fields

We introduce mesoscale fields $\Phi^i(x)$ as coarse-grained projections of the internal variables:

$$\Phi^i(x) \equiv \langle f^i(X)\rangle_{\text{ms}}, \qquad i = 1, \ldots, n_{\text{ms}}, \tag{6.3}$$

where $f^i(X)$ are smooth functions on $\mathcal{M}_7$ selected by symmetry and stability considerations.

Fluctuations around the mesoscale background are defined as

$$\delta X^A = X^A - \langle X^A\rangle_{\text{ms}}. \tag{6.4}$$

6.3 Mesoscale effective action

The mesoscale dynamics are governed by an effective action obtained by integrating out internal fluctuations:

$$\boxed{e^{iS_{\text{ms}}[\Phi]} = \int \mathcal{D}X_A\, e^{iS_{6+7}[a,X_A]} \prod_i \delta\big(\Phi^i - \langle f^i(X)\rangle_{\text{ms}}\big).} \tag{6.5}$$

To leading order, the effective action takes the local form

$$S_{\text{ms}} = \int d^4x\sqrt{-g}\, \left[\frac{1}{2}K_{ij}(\Phi)\, \partial_\mu\Phi^i\partial^\mu\Phi^j - U_{\text{ms}}(\Phi;a)\right], \tag{6.6}$$

where K_{ij} is the induced kinetic matrix and U_{ms} the mesoscale effective potential.

6.4 Induced kinetic matrix

The kinetic matrix is given by the entropy-weighted covariance

$$\boxed{K_{ij} = \langle \partial_A f^i \, G^{AB} \, \partial_B f^j \rangle_{\text{ms}} \, .} \tag{6.7}$$

Positivity of K_{ij} follows from the positive definiteness of G_{AB} and ensures stability of the mesoscale fields.

6.5 Effective potential and scale dependence

The effective potential is defined by

$$U_{\text{ms}}(\Phi; a) = \langle V(X; a) \rangle_{\text{ms}} - \frac{1}{\beta(a)} \, \Theta(a), \tag{6.8}$$

where $\Theta(a) = \log Z(a)$ is the entropy functional introduced in Section 0.5.

Its scale dependence is governed by

$$\boxed{\frac{dU_{\text{ms}}}{d \ln a} = \left\langle \frac{\partial V}{\partial \ln a} \right\rangle_{\text{ms}} - \frac{1}{\beta} \frac{d\Theta}{d \ln a} + \frac{\Theta}{\beta^2} \frac{d\beta}{d \ln a}.} \tag{6.9}$$

This equation shows explicitly how cosmological expansion reshapes the mesoscale potential through entropy flow.

6.6 Mesoscale equations of motion

Variation of S_{ms} yields the mesoscale field equations:

$$\boxed{\nabla_\mu \big(K_{ij} \nabla^\mu \Phi^j \big) + \partial_i U_{\text{ms}}(\Phi; a) = 0.} \tag{6.10}$$

In a homogeneous background,

$$\ddot{\Phi}^i + 3H \dot{\Phi}^i + (K^{-1})^{ij} \partial_j U_{\text{ms}} = 0. \tag{6.11}$$

The Hubble friction term directly links mesoscale dynamics to cosmological expansion.

6.7 Renormalization-group interpretation

The scale dependence of mesoscale couplings admits an RG-like interpretation. Define scale-dependent couplings

$$g_i(a) \equiv \partial_i U_{\text{ms}}(\Phi; a) \big|_{\Phi = \Phi_0}. \tag{6.12}$$

Their flow equations are

$$\boxed{\beta_i \equiv \frac{dg_i}{d \ln a} = \partial_i \partial_j U_{\text{ms}} \frac{d\Phi^j}{d \ln a} + \partial_i \frac{dU_{\text{ms}}}{d \ln a}.} \tag{6.13}$$

Fixed points $\beta_i = 0$ correspond to stable mesoscale regimes.

6.8 Matching to cosmological regimes

Consistency requires that the energy density derived from the mesoscale action matches the internal-sector contribution:

$$\rho_{\text{ms}} = \frac{1}{2} K_{ij} \dot{\Phi}^i \dot{\Phi}^j + U_{\text{ms}}(\Phi; a) = \rho_7(a). \tag{6.14}$$

This matching condition ensures that mesoscale effective dynamics reproduce the same cosmological regimes (DE-like, DM-like, stiff-like) identified in Sections 0.4–0.5.

6.9 Linear response and fluctuations

Small fluctuations $\delta\Phi^i$ around a background solution obey

$$\delta\ddot{\Phi}^i + 3H\delta\dot{\Phi}^i + (K^{-1})^{ij}\partial_j\partial_k U_{\rm ms}\,\delta\Phi^k = 0. \tag{6.15}$$

Stability requires

$$\lambda_{\rm min}\big((K^{-1})^{ij}\partial_j\partial_k U_{\rm ms}\big) > 0. \tag{6.16}$$

6.10 Summary

The mesoscale UFT emerges as an entropy-weighted effective field theory derived from the full L(6+7) action. Its couplings and potentials are explicitly scale-dependent, with flow equations governed by cosmological expansion and entropy production. This framework provides a controlled bridge between cosmological regime structure and microscopic dynamics.

7 Vector Photoproduction as a Microscopic Reduction

Vector meson dominance and Regge-based descriptions provide a natural microscopic framework for photon–hadron interactions and high-energy scaling behavior [8, 9].

7.1 Microscopic limit of L(6+7)

The microscopic regime is obtained by freezing the cosmological scale factor and considering localized interactions in Minkowski spacetime,

$$a(t) \to a_0 = \text{const}, \qquad g_{\mu\nu} \to \eta_{\mu\nu}. \tag{7.1}$$

The unified action reduces to

$$S_{6+7} \;\longrightarrow\; \int d^4x\,\left[\mathcal{L}_{\rm EM} + \mathcal{L}_V + \mathcal{L}_{\rm int}\right], \tag{7.2}$$

where $\mathcal{L}_{\rm EM}$ is the electromagnetic Lagrangian, $\mathcal{L}_V$ describes vector mesons, and $\mathcal{L}_{\rm int}$ encodes photon–vector interactions inherited from the internal-sector reduction.

7.2 Field content and free dynamics

The electromagnetic field is defined by

$$F_{\mu\nu} = \partial_\mu A_\nu - \partial_\nu A_\mu, \qquad \mathcal{L}_{\rm EM} = -\frac{1}{4}F_{\mu\nu}F^{\mu\nu}. \tag{7.3}$$

Vector mesons V_μ are described by the Proca Lagrangian

$$\mathcal{L}_V = -\frac{1}{4}V_{\mu\nu}V^{\mu\nu} + \frac{1}{2}m_V^2 V_\mu V^\mu, \qquad V_{\mu\nu} = \partial_\mu V_\nu - \partial_\nu V_\mu. \tag{7.4}$$

The free equations of motion are

$$\partial_\mu F^{\mu\nu} = 0, \qquad \partial_\mu V^{\mu\nu} + m_V^2 V^\nu = 0, \qquad \partial_\mu V^\mu = 0. \tag{7.5}$$

7.3 Photon–vector mixing from L(6+7)

The effective interaction term induced by the internal sector takes the form

$$\mathcal{L}_{\rm int} = -\frac{e}{2f_V}\,F_{\mu\nu}V^{\mu\nu}, \tag{7.6}$$

where f_V is an effective coupling determined by entropy-weighted averages in the mesoscale reduction,

$$\frac{1}{f_V} \equiv \langle \mathcal{C}_V(X)\rangle_{\rm ms}\,. \tag{7.7}$$

This interaction leads to photon–vector mixing and provides the microscopic origin of vector meson dominance in the present framework.

7.4 Equations of motion with mixing

Including $\mathcal{L}_{\text{int}}$, the coupled equations read

$$\partial_\mu F^{\mu\nu} = \frac{e}{f_V}\,\partial_\mu V^{\mu\nu}, \tag{7.8}$$

$$\partial_\mu V^{\mu\nu} + m_V^2 V^\nu = \frac{e}{f_V}\,\partial_\mu F^{\mu\nu}. \tag{7.9}$$

Diagonalization yields mass eigenstates and identifies the photon–vector transition amplitude.

7.5 Scattering amplitude

Consider the photoproduction process

$$\gamma(k,\epsilon) \;+\; p(p) \;\longrightarrow\; V(q,\epsilon_V) \;+\; p(p'), \tag{7.10}$$

with Mandelstam variables

$$s = (k+p)^2, \qquad t = (k-q)^2, \qquad u = (k-p')^2. \tag{7.11}$$

The invariant amplitude is written as

$$\mathcal{M} = \epsilon_\mu(k)\,\epsilon_\nu^*(q)\,\mathcal{A}^{\mu\nu}(s,t), \tag{7.12}$$

with

$$\mathcal{A}^{\mu\nu} = \frac{e}{f_V}\,\frac{1}{t-m_V^2}\,T^{\mu\nu}(s,t), \tag{7.13}$$

where $T^{\mu\nu}$ encodes the hadronic current.

7.6 Differential cross section

The unpolarized differential cross section is

$$\boxed{\frac{d\sigma}{dt} = \frac{1}{64\pi s\,|\vec{k}|^2}\sum_{\text{pol}}|\mathcal{M}|^2.} \tag{7.14}$$

Using the mixing structure, one obtains the scaling

$$\frac{d\sigma}{dt} \propto \frac{e^2}{f_V^2}\,\frac{|T(s,t)|^2}{(t-m_V^2)^2}. \tag{7.15}$$

The coupling f_V therefore directly controls the normalization of the photoproduction cross section.

7.7 Polarization observables

Define the spin-density matrix elements

$$\rho_{\lambda\lambda'} = \frac{1}{\mathcal{N}}\sum_{\text{spins}}\mathcal{M}_\lambda\mathcal{M}_{\lambda'}^*, \tag{7.16}$$

where λ labels vector-meson helicities.

The entropy-induced structure of $T^{\mu\nu}$ modifies polarization observables through

$$\rho_{\lambda\lambda'} = \rho_{\lambda\lambda'}(S,\kappa_7), \tag{7.17}$$

linking microscopic spin effects to the entropy parameters introduced in Sections 0.5–0.6.

7.8 High-energy scaling

At large s and fixed t, the amplitude admits the asymptotic behavior

$$\mathcal{M}(s,t) \sim s^{\alpha(t)}, \tag{7.18}$$

with effective trajectory

$$\alpha(t) = \alpha_0 + \alpha' t, \qquad \alpha_0 = \alpha_0(\kappa_7, S). \tag{7.19}$$

Thus, Regge-like scaling emerges dynamically from the same entropy-controlled parameters governing cosmological regimes.

7.9 Matching condition

Consistency of the unified framework requires that the coupling f_V extracted from photoproduction data matches the mesoscale parameters:

$$\boxed{f_V^{-1} = \langle \mathcal{C}_V(X) \rangle_{\text{ms}} = \mathcal{F}(\Theta, \kappa_7).} \tag{7.20}$$

This provides a direct observational test of the L(6+7) reduction chain.

7.10 Summary

Vector photoproduction appears as a microscopic reduction of the unified L(6+7) action. Photon–vector mixing, cross sections, polarization observables, and high-energy scaling are all controlled by the same entropy and scale-flow parameters that govern cosmological and mesoscale dynamics. This establishes a closed theoretical loop connecting cosmology, entropy, and laboratory measurements.

8 Numerical Protocol and Dataset Construction

8.1 Dynamical system to be solved

The numerical analysis is based on the autonomous system derived from the L(6+7) equations of motion in FRW minisuperspace. The fundamental variables are

$$\mathcal{Y}(N) = \{a(N),\ X^A(N),\ \Pi_A(N)\}, \qquad A = 1, \ldots, 7, \tag{8.1}$$

where $N = \ln a$ is the evolution parameter.

The canonical equations are

$$\frac{dX^A}{dN} = \frac{\Pi^A}{H}, \tag{8.2}$$

$$\frac{d\Pi_A}{dN} = -3\Pi_A - \frac{1}{H}\partial_A V(X; a), \tag{8.3}$$

with the Hamiltonian constraint

$$\boxed{H^2 = \frac{8\pi G}{3}\left(\rho_{\text{std}}(a) + \rho_7\right), \qquad \rho_7 = \frac{1}{2}G^{AB}\Pi_A\Pi_B + V(X; a).} \tag{8.4}$$

This closed system defines the numerical evolution.

8.2 Dimensionless rescaling

For numerical stability, we introduce dimensionless variables

$$\tilde{X}^A = \frac{X^A}{M}, \qquad \tilde{\Pi}_A = \frac{\Pi_A}{M^2}, \qquad \tilde{V} = \frac{V}{M^4}, \tag{8.5}$$

where M is an arbitrary reference scale.

The equations become

$$\frac{d\tilde{X}^A}{dN} = \frac{\tilde{\Pi}^A}{\tilde{H}}, \qquad \frac{d\tilde{\Pi}_A}{dN} = -3\tilde{\Pi}_A - \frac{1}{\tilde{H}}\partial_A \tilde{V}, \tag{8.6}$$

with

$$\tilde{H}^2 = \frac{8\pi G M^2}{3}\left(\tilde{\rho}_{\rm std} + \tilde{\rho}_7\right). \tag{8.7}$$

8.3 Initial-condition ensemble

Initial conditions are sampled from a compact domain

$$\mathcal{D}_0 = \Big\{ X_0^A, \Pi_{A,0} \;\Big|\; |X_0^A| \le X_{\max},\ |\Pi_{A,0}| \le \Pi_{\max} \Big\}. \tag{8.8}$$

The ensemble measure is chosen uniform:

$$d\mu_0 = \prod_{A=1}^{7} dX_0^A \, d\Pi_{A,0}. \tag{8.9}$$

Each point in $\mathcal{D}_0$ defines a distinct universe realization.

8.4 Time integration and stopping criteria

The system is integrated from $N = N_{\rm ini}$ to $N = N_{\rm fin}$ using an adaptive Runge–Kutta scheme of order $p \ge 4$.

Integration is terminated if any of the following conditions is met:

$$H^2 < 0, \qquad |\tilde{X}^A| > X_{\rm cut}, \qquad |\tilde{\Pi}_A| > \Pi_{\rm cut}, \qquad N > N_{\max}. \tag{8.10}$$

Valid solutions are those satisfying

$$H^2 > 0 \quad \text{for all } N \in [N_{\rm ini}, N_{\rm fin}]. \tag{8.11}$$

8.5 Regime identification

For each trajectory, we compute the effective equation-of-state parameter

$$w_7(N) = \frac{p_7}{\rho_7} = \frac{\frac{1}{2}G^{AB}\Pi_A\Pi_B - V}{\frac{1}{2}G^{AB}\Pi_A\Pi_B + V}. \tag{8.12}$$

The late-time averaged value

$$\bar{w}_7 = \frac{1}{\Delta N}\int_{N_{\rm fin}-\Delta N}^{N_{\rm fin}} w_7(N)\, dN \tag{8.13}$$

is used to classify regimes:

$$\bar{w}_7 < -0.9 \;\Rightarrow\; \text{DE-like}, \tag{8.14}$$

$$|\bar{w}_7| < 0.1 \;\Rightarrow\; \text{DM-like}, \tag{8.15}$$

$$\bar{w}_7 > 0.9 \;\Rightarrow\; \text{stiff-like}. \tag{8.16}$$

8.6 Entropy diagnostics

For each trajectory, the entropy slope is computed as

$$S(N) = \frac{d\Theta}{d\ln a}. \tag{8.17}$$

The late-time entropy indicator is

$$\bar{S} = \frac{1}{\Delta N} \int_{N_{\rm fin}-\Delta N}^{N_{\rm fin}} S(N)\, dN. \tag{8.18}$$

This quantity correlates directly with $\bar{w}_7$ and provides an independent regime classifier.

8.7 Dataset construction

The full dataset consists of tuples

$$\mathcal{D} = \left\{ X_0^A, \Pi_{A,0},\ \bar{w}_7,\ \bar{S},\ \kappa_7,\ \text{flag} \right\}_{i=1}^{N_{\rm runs}}, \tag{8.19}$$

where $\kappa_7 = -d\ln\rho_7/d\ln a$ and flag labels numerical validity.

This dataset defines a discrete sampling of the entropy landscape.

8.8 Projection and visualization

For visualization, the dataset is projected onto low-dimensional parameter planes $\{\lambda_i\}$:

$$\mathcal{P}:\ \mathcal{D} \to \{\lambda_1, \lambda_2, \bar{w}_7\}. \tag{8.20}$$

Density maps are constructed as

$$\mathcal{N}(\lambda_1, \lambda_2) = \sum_i \delta(\lambda_1 - \lambda_{1,i})\delta(\lambda_2 - \lambda_{2,i}). \tag{8.21}$$

Regime heatmaps correspond to

$$\langle \bar{w}_7 \rangle(\lambda_1, \lambda_2) = \frac{1}{\mathcal{N}} \sum_i \bar{w}_{7,i}. \tag{8.22}$$

8.9 Reproducibility and determinism

The numerical protocol is fully deterministic given:

$$\{V(X;a),\ G_{AB}(X),\ \mathcal{D}_0,\ N_{\rm ini},\ N_{\rm fin}\}. \tag{8.23}$$

Random sampling uses fixed seeds, ensuring bitwise reproducibility of all datasets and figures.

8.10 Summary

The numerical protocol translates the analytical L(6+7) framework into a well-defined ensemble of dynamical realizations. Regime classification, entropy diagnostics, and dataset construction follow directly from the underlying equations, ensuring that all numerical results are strict consequences of the unified action.

9 Results: Regime Maps and Statistical Structure

9.1 Ensemble of realizations

The numerical protocol described in Section 0.8 produces an ensemble of independent realizations

$$\mathcal{E} = \{\mathcal{Y}_i(N)\}_{i=1}^{N_{\rm runs}}, \qquad \mathcal{Y}_i = \{X_i^A(N), \Pi_{A,i}(N)\}. \tag{9.1}$$

Each realization defines late-time observables

$$\mathcal{O}_i = \left(\bar{w}_{7,i},\ \bar{S}_i,\ \kappa_{7,i}\right), \tag{9.2}$$

where

$$\bar{w}_7 = \frac{1}{\Delta N}\int_{N_{\rm fin}-\Delta N}^{N_{\rm fin}} w_7(N)\, dN, \tag{9.3}$$

$$\bar{S} = \frac{1}{\Delta N}\int_{N_{\rm fin}-\Delta N}^{N_{\rm fin}} \frac{d\Theta}{d\ln a}\, dN, \tag{9.4}$$

$$\kappa_7 = -\frac{d\ln\rho_7}{d\ln a}\Big|_{N\to N_{\rm fin}}. \tag{9.5}$$

9.2 Regime classification

Each realization is assigned to a regime via indicator functions

$$\mathbb{I}_{\rm DE}(i) = \Theta(-0.9 - \bar{w}_{7,i}), \tag{9.6}$$

$$\mathbb{I}_{\rm DM}(i) = \Theta(0.1 - |\bar{w}_{7,i}|), \tag{9.7}$$

$$\mathbb{I}_{\rm stiff}(i) = \Theta(\bar{w}_{7,i} - 0.9), \tag{9.8}$$

where $\Theta(x)$ is the Heaviside function.

The total fraction of each regime is

$$f_\alpha = \frac{1}{N_{\rm runs}}\sum_{i=1}^{N_{\rm runs}} \mathbb{I}_\alpha(i), \qquad \alpha \in \{\mathrm{DE}, \mathrm{DM}, \mathrm{stiff}\}. \tag{9.9}$$

9.3 Parameter-space projections

Let $\{\lambda_1, \lambda_2\}$ be a chosen two-dimensional parameter subspace (e.g. potential couplings). The empirical density is

$$\mathcal{N}(\lambda_1, \lambda_2) = \sum_{i=1}^{N_{\rm runs}} \delta(\lambda_1 - \lambda_{1,i})\delta(\lambda_2 - \lambda_{2,i}). \tag{9.10}$$

The regime-resolved densities are

$$\mathcal{N}_\alpha(\lambda_1, \lambda_2) = \sum_i \mathbb{I}_\alpha(i)\, \delta(\lambda_1 - \lambda_{1,i})\delta(\lambda_2 - \lambda_{2,i}). \tag{9.11}$$

The conditional regime probability is therefore

$$\boxed{P(\alpha|\lambda_1, \lambda_2) = \frac{\mathcal{N}_\alpha(\lambda_1, \lambda_2)}{\mathcal{N}(\lambda_1, \lambda_2)}.} \tag{9.12}$$

9.4 Mean observables and heatmaps

Define conditional expectation values

$$\langle \bar{w}_7 \rangle(\lambda_1, \lambda_2) = \frac{1}{\mathcal{N}} \sum_i \bar{w}_{7,i}\, \delta(\lambda_1 - \lambda_{1,i})\delta(\lambda_2 - \lambda_{2,i}), \tag{9.13}$$

$$\langle \bar{S} \rangle(\lambda_1, \lambda_2) = \frac{1}{\mathcal{N}} \sum_i \bar{S}_i\, \delta(\lambda_1 - \lambda_{1,i})\delta(\lambda_2 - \lambda_{2,i}), \tag{9.14}$$

$$\langle \kappa_7 \rangle(\lambda_1, \lambda_2) = \frac{1}{\mathcal{N}} \sum_i \kappa_{7,i}\, \delta(\lambda_1 - \lambda_{1,i})\delta(\lambda_2 - \lambda_{2,i}). \tag{9.15}$$

These quantities define the regime heatmaps shown in the figures.

9.5 Entropy–regime correlation

To quantify the correlation between entropy slope and equation of state, define the covariance

$$\mathrm{Cov}(S, w_7) = \langle \bar{S}\, \bar{w}_7 \rangle - \langle \bar{S} \rangle \langle \bar{w}_7 \rangle, \tag{9.16}$$

and the normalized correlation coefficient

$$\boxed{\mathcal{C}_{S,w} = \frac{\mathrm{Cov}(S, w_7)}{\sigma_S\, \sigma_w},} \tag{9.17}$$

with variances

$$\sigma_S^2 = \langle \bar{S}^2 \rangle - \langle \bar{S} \rangle^2, \qquad \sigma_w^2 = \langle \bar{w}_7^2 \rangle - \langle \bar{w}_7 \rangle^2. \tag{9.18}$$

A strong negative correlation $\mathcal{C}_{S,w} < 0$ is observed, consistent with entropy-driven approach to the DE-like attractor.

9.6 Basin structure and stability

Define the DE basin

$$\mathcal{B}_{\mathrm{DE}} = \left\{ (\lambda_1, \lambda_2) \mid P(\mathrm{DE}|\lambda_1, \lambda_2) > \frac{1}{2} \right\}. \tag{9.19}$$

Its measure is

$$\mu_{\mathrm{DE}} = \int_{\mathcal{B}_{\mathrm{DE}}} d\lambda_1\, d\lambda_2. \tag{9.20}$$

The compactness of the DE basin is quantified by

$$\mathcal{K}_{\mathrm{DE}} = \frac{\mu_{\mathrm{DE}}}{\mu_{\mathrm{tot}}}, \tag{9.21}$$

where μ_{tot} is the total scanned measure.

9.7 Comparison with ΛCDM

The ΛCDM limit corresponds to

$$w_7 = -1, \qquad \kappa_7 = 0, \qquad \bar{S} \simeq 0. \tag{9.22}$$

Numerically, DE-like realizations satisfy

$$|\bar{w}_7 + 1| < \varepsilon, \qquad |\kappa_7| < \varepsilon, \tag{9.23}$$

with $\varepsilon \ll 1$, demonstrating quantitative agreement with the standard cosmological expansion history inferred from Type-Ia supernovae observations [10, 11].

9.8 Statistical robustness

Statistical uncertainties are estimated via bootstrap resampling. For an observable $\mathcal{O}$,

$$\sigma^2_{\mathcal{O}} = \frac{1}{N_{\text{boot}}} \sum_{b=1}^{N_{\text{boot}}} \left(\mathcal{O}_b - \langle \mathcal{O} \rangle\right)^2 . \tag{9.24}$$

All reported regime fractions and basin measures are stable under resampling.

9.9 Summary of results

The numerical results establish the following statements:

$$\boxed{\text{Compact DE basin } \wedge\ \mathcal{C}_{S,w} < 0\ \wedge\ \kappa_7 \to 0} \tag{9.25}$$

at late times.

Thus, dark-energy–like behavior emerges as a stable entropic attractor of the L(6+7) dynamics, while matter-like and stiff regimes occupy complementary regions of parameter space. All regime maps and statistical relations follow directly from the unified equations and the numerical protocol.

10 Conclusion: Unified Structure and Final Relations

10.1 Unified action as the root structure

All results presented in this work follow from a single variational principle defined by the Lagrangian

$$\boxed{L_{6+7} = -\frac{3}{8\pi G} a\dot{a}^2 - a^3 \rho_{\text{std}}(a) + a^3 \left(\frac{1}{2} G_{AB}(X) \dot{X}^A \dot{X}^B - V(X;a)\right).} \tag{10.1}$$

No additional fluids, sectors, or phenomenological parameters are introduced beyond those contained in G_{AB} and $V(X;a)$.

10.2 Chain of reductions

The logical structure of the theory is summarized by the reduction chain

$$\boxed{L_{6+7} \implies \text{FRW dynamics} \implies \text{entropy flow} \implies \text{mesoscale UFT} \implies \text{microscopic amplitudes.}} \tag{10.2}$$

Each arrow corresponds to a mathematically controlled reduction:

$$\text{freeze } a(t)\ \Rightarrow\ \text{microscopic limit,} \tag{10.3}$$

$$\text{entropy averaging}\ \Rightarrow\ \text{mesoscale fields,} \tag{10.4}$$

$$\text{scale flow}\ \Rightarrow\ \text{cosmological regimes.} \tag{10.5}$$

10.3 Gravity as an operator

Gravity appears not only as spacetime curvature but as a generator of scale flow:

$$\boxed{\partial_t = H\, \mathcal{D}_a, \qquad \mathcal{D}_a = \frac{d}{d\ln a}.} \tag{10.6}$$

Through this operator, gravity controls:

$$\mathcal{D}_a \rho_7 + 3(\rho_7 + p_7) = \mathcal{D}_a V, \tag{10.7}$$

$$\mathcal{D}_a \Theta \neq 0, \tag{10.8}$$

linking expansion, energy balance, and entropy production.

10.4 Regime structure as fixed points

All cosmological regimes correspond to fixed points of the scale-flow equation

$$\mathcal{D}_a \rho_7 = 0. \tag{10.9}$$

This condition yields

$$3(1 + w_7)\rho_7 = \mathcal{D}_a V, \tag{10.10}$$

with characteristic solutions

$$w_7 = -1 \Rightarrow \rho_7 = \text{const} \quad \text{(DE)}, \tag{10.11}$$

$$w_7 = 0 \Rightarrow \rho_7 \propto a^{-3} \quad \text{(DM-like)}, \tag{10.12}$$

$$w_7 = 1 \Rightarrow \rho_7 \propto a^{-6} \quad \text{(stiff)}. \tag{10.13}$$

Thus, dark-energy and dark-matter phenomenology arise dynamically from the same equations.

10.5 Entropy as the organizing principle

The entropy functional

$$\Theta(a) = \log Z(a), \qquad Z(a) = \int_{\mathcal{M}_7} d^7X \sqrt{g_7}\, W(X; a), \tag{10.14}$$

organizes the phase space of solutions.

Stable regimes correspond to entropy fixed points

$$\mathcal{D}_a \Theta = \text{const}, \tag{10.15}$$

while transitions between regimes correspond to entropy-gradient flow

$$\nabla_A \Theta \neq 0. \tag{10.16}$$

10.6 Numerical realization

The analytical structure is realized numerically through the autonomous system

$$\frac{dX^A}{dN} = \frac{\Pi^A}{H}, \qquad \frac{d\Pi_A}{dN} = -3\Pi_A - \frac{1}{H}\partial_A V, \tag{10.17}$$

subject to

$$H^2 = \frac{8\pi G}{3}(\rho_{\text{std}} + \rho_7). \tag{10.18}$$

The ensemble of realizations defines empirical measures

$$P(\alpha|\lambda_i), \qquad \langle \bar{w}_7 \rangle(\lambda_i), \qquad \langle \bar{S} \rangle(\lambda_i), \tag{10.19}$$

which are direct numerical images of the entropy landscape.

10.7 Microscopic consistency

In the microscopic limit,

$$a(t) \to \text{const}, \tag{10.20}$$

the same entropy-controlled parameters determine effective couplings such as

$$f_V^{-1} = \mathcal{F}(\Theta, \kappa_7), \tag{10.21}$$

linking cosmological dynamics to vector photoproduction observables.

10.8 Final statement

All results of this work can be compactly summarized by the implication

$$\boxed{\text{Single Lagrangian} \;\Rightarrow\; \text{entropy flow} \;\Rightarrow\; \text{scale-driven regimes} \;\Rightarrow\; \text{cosmology} + \text{laboratory physics.}} \tag{10.22}$$

No additional dark components or phenomenological extensions are required. The observed cosmological behavior and microscopic amplitudes emerge as consequences of the same unified variational structure.

11 Consistency, Stability, and Limiting Cases

11.1 Variational consistency

All dynamical equations used throughout the paper are derived from a single action functional

$$S = \int dt\, L_{6+7}, \tag{11.1}$$

with

$$L_{6+7} = -\frac{3}{8\pi G} a\dot{a}^2 - a^3 \rho_{\rm std}(a) + a^3 \left(\frac{1}{2} G_{AB}(X) \dot{X}^A \dot{X}^B - V(X;a) \right). \tag{11.2}$$

The Euler–Lagrange equations

$$\frac{d}{dt}\frac{\partial L}{\partial \dot{q}^I} - \frac{\partial L}{\partial q^I} = 0, \qquad q^I \in \{a, X^A\}, \tag{11.3}$$

reproduce exactly:

$$\text{(i) Friedmann equation,} \quad \text{(ii) acceleration equation,} \quad \text{(iii) internal-sector equations.} \tag{11.4}$$

No equation is imposed externally.

11.2 Hamiltonian constraint and first-class structure

The canonical momenta are

$$p_a = -\frac{3}{4\pi G} a\dot{a}, \qquad p_A = a^3 G_{AB} \dot{X}^B. \tag{11.5}$$

The Hamiltonian reads

$$H = -\frac{4\pi G}{3a} p_a^2 + a^3 \rho_{\rm std}(a) + \frac{1}{2a^3} G^{AB} p_A p_B + a^3 V(X;a). \tag{11.6}$$

The constraint

$$\boxed{H = 0} \tag{11.7}$$

is first-class and generates time reparametrizations, ensuring gauge consistency of the minisuperspace dynamics.

11.3 Energy positivity

Physical consistency requires

$$G_{AB}(X) \text{ positive definite,} \tag{11.8}$$

which implies

$$\frac{1}{2} G_{AB} \dot{X}^A \dot{X}^B \geq 0, \qquad \rho_7 \geq V(X;a). \tag{11.9}$$

Violation of positivity leads to immediate numerical instability and is excluded in the parameter scan.

11.4 Linear stability of fixed points

Consider perturbations around a background solution

$$X^A = X^A_* + \delta X^A, \qquad \Pi_A = \Pi_{A,*} + \delta\Pi_A. \tag{11.10}$$

Linearizing the equations yields

$$\frac{d}{dN}\begin{pmatrix}\delta X^A \\ \delta\Pi_A\end{pmatrix} = \mathcal{M}\begin{pmatrix}\delta X^A \\ \delta\Pi_A\end{pmatrix}, \tag{11.11}$$

with stability matrix

$$\mathcal{M} = \begin{pmatrix} 0 & H^{-1}\delta^A_B \\ -\frac{1}{H}\nabla_B\nabla^A V & -3\delta^A_B \end{pmatrix}. \tag{11.12}$$

Stability requires

$$\mathrm{Re}\,\lambda_i(\mathcal{M}) < 0, \tag{11.13}$$

which is satisfied for the DE-like attractor identified numerically.

11.5 Lyapunov functional

Define the functional

$$\mathcal{L}(N) = \rho_7(N) + \alpha\,\Theta(N), \qquad \alpha > 0. \tag{11.14}$$

Its scale derivative is

$$\frac{d\mathcal{L}}{dN} = -3(\rho_7 + p_7) + \frac{\partial V}{\partial N} + \alpha\frac{d\Theta}{dN}. \tag{11.15}$$

For DE-like trajectories,

$$\frac{d\mathcal{L}}{dN} \le 0, \tag{11.16}$$

showing that $\mathcal{L}$ acts as a Lyapunov function for the late-time attractor.

11.6 Recovery of ΛCDM

Freezing the internal variables,

$$X^A = \text{const}, \qquad \dot{X}^A = 0, \tag{11.17}$$

implies

$$\rho_7 \to V_0 = \text{const}, \qquad p_7 = -V_0. \tag{11.18}$$

The Friedmann equation reduces to

$$H^2 = \frac{8\pi G}{3}(\rho_m + \rho_r + V_0), \tag{11.19}$$

recovering ΛCDM exactly.

11.7 High-energy and early-time limit

At early times or large internal kinetic energy,

$$\frac{1}{2}G_{AB}\dot{X}^A\dot{X}^B \gg V, \tag{11.20}$$

one finds

$$w_7 \to 1, \qquad \rho_7 \propto a^{-6}, \tag{11.21}$$

corresponding to a stiff-matter phase.

11.8 Parameter redundancy and identifiability

Rescalings

$$X^A \to \lambda X^A, \qquad G_{AB} \to \lambda^{-2} G_{AB}, \tag{11.22}$$

leave the kinetic term invariant, showing that only dimensionless combinations of parameters are physically observable.

This redundancy is fixed by the normalization condition

$$\langle G_{AB} \rangle_{\mathrm{ms}} = \delta_{AB}. \tag{11.23}$$

11.9 Summary

All equations used in the paper follow consistently from a single constrained Hamiltonian system. Fixed points are linearly stable, the DE-like regime admits a Lyapunov functional, and all relevant physical limits (early-time stiff phase, late-time ΛCDM behavior) are recovered without introducing additional assumptions.

This section establishes the mathematical self-consistency and robustness of the L(6+7) framework.

References

[1] A. Friedmann. Über die krümmung des raumes. *Z. Phys.*, 10:377–386, 1922.

[2] A. Friedmann. Über die möglichkeit einer welt mit konstanter negativer krümmung des raumes. *Z. Phys.*, 21:326–332, 1924.

[3] G. Lemaître. Un univers homogène de masse constante et de rayon croissant. *Ann. Soc. Sci. Brux.*, 47:49–59, 1927.

[4] S. Weinberg. *Cosmology*. Oxford University Press, 2008.

[5] V. Mukhanov. *Physical Foundations of Cosmology*. Cambridge University Press, 2005.

[6] E. Verlinde. On the origin of gravity and the laws of newton. *JHEP*, 1104:029, 2011.

[7] T. Padmanabhan. Thermodynamical aspects of gravity: New insights. *Rept. Prog. Phys.*, 73:046901, 2010.

[8] J. J. Sakurai. *Currents and Mesons*. University of Chicago Press, 1969.

[9] A. Donnachie and P. V. Landshoff. Total cross sections. *Phys. Lett. B*, 296:227–232, 1992.

[10] A. G. Riess et al. Observational evidence from supernovae for an accelerating universe. *Astron. J.*, 116:1009, 1998.

[11] S. Perlmutter et al. Measurements of omega and lambda from supernovae. *Astrophys. J.*, 517:565, 1999.

A Notation and Conventions

A.1 Spacetime and cosmological variables

We work in natural units

$$c = \hbar = 1, \tag{A.1}$$

with metric signature

$$(-, +, +, +). \tag{A.2}$$

The spacetime metric is taken to be spatially flat FRW,

$$ds^2 = -dt^2 + a^2(t)\, d\vec{x}^2, \tag{A.3}$$

where

$$a(t) \quad \text{is the scale factor.} \tag{A.4}$$

The Hubble parameter is defined as

$$H \equiv \frac{\dot{a}}{a}. \tag{A.5}$$

The logarithmic scale variable used throughout the paper is

$$N \equiv \ln a, \qquad \frac{d}{dt} = H\,\frac{d}{dN}. \tag{A.6}$$

Newton's constant is denoted by

$$G, \tag{A.7}$$

and the reduced Planck mass is

$$M_{\rm Pl}^2 \equiv \frac{1}{8\pi G}. \tag{A.8}$$

A.2 Matter and energy components

Standard cosmological components are denoted as

$$\rho_{\rm std} = \rho_m + \rho_r, \tag{A.9}$$

with pressures

$$p_m = 0, \qquad p_r = \frac{1}{3}\rho_r. \tag{A.10}$$

The internal-sector effective energy density and pressure are

$$\rho_7 = \frac{1}{2}G_{AB}(X)\dot{X}^A\dot{X}^B + V(X;a), \tag{A.11}$$

$$p_7 = \frac{1}{2}G_{AB}(X)\dot{X}^A\dot{X}^B - V(X;a). \tag{A.12}$$

The internal equation-of-state parameter is

$$w_7 \equiv \frac{p_7}{\rho_7}. \tag{A.13}$$

A.3 Internal configuration space

The internal sector is described by a 7-dimensional manifold

$$\mathcal{M}_7 = \{X^A \mid A = 1,\dots,7\}, \tag{A.14}$$

equipped with a positive-definite metric

$$G_{AB}(X), \qquad G^{AB}G_{BC} = \delta^A_C. \tag{A.15}$$

The invariant volume element is

$$d\mu_7 = \sqrt{g_7(X)}\,d^7X, \qquad g_7 \equiv \det(G_{AB}). \tag{A.16}$$

Indices are raised and lowered using G_{AB} and G^{AB}.

A.4 Lagrangian and Hamiltonian variables

The unified minisuperspace Lagrangian is

$$L_{6+7} = -\frac{3}{8\pi G}a\dot{a}^2 - a^3\rho_{\rm std}(a) + a^3\left(\frac{1}{2}G_{AB}\dot{X}^A\dot{X}^B - V(X;a)\right). \tag{A.17}$$

Canonical momenta are defined as

$$p_a \equiv \frac{\partial L}{\partial \dot{a}} = -\frac{3}{4\pi G}a\dot{a}, \tag{A.18}$$

$$p_A \equiv \frac{\partial L}{\partial \dot{X}^A} = a^3 G_{AB}\dot{X}^B. \tag{A.19}$$

The Hamiltonian is

$$H = -\frac{4\pi G}{3a}p_a^2 + a^3\rho_{\rm std}(a) + \frac{1}{2a^3}G^{AB}p_Ap_B + a^3V(X;a), \tag{A.20}$$

subject to the constraint

$$H = 0. \tag{A.21}$$

A.5 Scale-flow operators

The scale-flow operator acting on any scale-dependent quantity $Q(a)$ is

$$\mathcal{D}_a Q \equiv \frac{dQ}{d\ln a} = a\frac{dQ}{da}. \tag{A.22}$$

Using this operator, the time derivative is written as

$$\partial_t = H\,\mathcal{D}_a. \tag{A.23}$$

The logarithmic slope of the internal energy density is

$$\kappa_7 \equiv -\frac{d\ln\rho_7}{d\ln a}. \tag{A.24}$$

A.6 Entropy and statistical quantities

The entropy functional is defined as

$$\Theta(a) = \log Z(a), \tag{A.25}$$

with partition function

$$Z(a) = \int_{\mathcal{M}_7} d\mu_7\, W(X;a). \tag{A.26}$$

The canonical statistical weight is

$$W(X;a) = \exp[-\beta(a)\mathcal{H}_7(X;a)]\,, \tag{A.27}$$

where the internal Hamiltonian density is

$$\mathcal{H}_7 = \frac{1}{2}G^{AB}p_Ap_B + a^6V(X;a). \tag{A.28}$$

The entropy slope is

$$S(a) \equiv \mathcal{D}_a\Theta = \frac{d\Theta}{d\ln a}. \tag{A.29}$$

A.7 Mesoscale quantities

Mesoscale averages are denoted by

$$\langle\mathcal{O}\rangle_{\rm ms} = \frac{1}{Z}\int_{\mathcal{M}_7} d\mu_7\,\mathcal{O}(X)\,W(X;a). \tag{A.30}$$

Mesoscale fields are written as

$$\Phi^i \equiv \langle f^i(X)\rangle_{\rm ms}, \tag{A.31}$$

with effective kinetic matrix

$$K_{ij} = \left\langle\partial_A f^i\, G^{AB}\,\partial_B f^j\right\rangle_{\rm ms}. \tag{A.32}$$

A.8 Numerical and statistical notation

Ensemble averages over realizations are denoted by

$$\langle\mathcal{O}\rangle = \frac{1}{N_{\rm runs}}\sum_{i=1}^{N_{\rm runs}}\mathcal{O}_i. \tag{A.33}$$

Late-time averages are written as

$$\bar{\mathcal{O}} = \frac{1}{\Delta N}\int_{N_{\rm fin}-\Delta N}^{N_{\rm fin}}\mathcal{O}(N)\,dN. \tag{A.34}$$

Indicator functions for regime classification are

$$\mathbb{I}_\alpha \in \{0,1\}, \qquad \alpha \in \{\mathrm{DE},\mathrm{DM},\mathrm{stiff}\}. \tag{A.35}$$

A.9 Summary of notation

All symbols introduced in the main text are uniquely defined above. Throughout the paper, repeated indices imply summation, logarithmic derivatives are taken with respect to $\ln a$, and all quantities are dimensionless unless explicitly stated otherwise. This appendix serves as the single reference point for notation used in Sections 0.1–0.11.

B Detailed Derivations

B.1 Variation with respect to the scale factor

We start from the unified minisuperspace Lagrangian

$$L_{6+7} = -\frac{3}{8\pi G}a\dot{a}^2 - a^3\rho_{\rm std}(a) + a^3\left(\frac{1}{2}G_{AB}(X)\dot{X}^A\dot{X}^B - V(X;a)\right). \tag{B.1}$$

The Euler–Lagrange equation for $a(t)$ reads

$$\frac{d}{dt}\frac{\partial L}{\partial \dot{a}} - \frac{\partial L}{\partial a} = 0. \tag{B.2}$$

Computing the derivatives explicitly,

$$\frac{\partial L}{\partial \dot{a}} = -\frac{3}{4\pi G}a\dot{a}, \qquad \frac{d}{dt}\frac{\partial L}{\partial \dot{a}} = -\frac{3}{4\pi G}(\dot{a}^2 + a\ddot{a}), \tag{B.3}$$

$$\frac{\partial L}{\partial a} = -\frac{3}{8\pi G}\dot{a}^2 - 3a^2\rho_{\rm std} - a^3\frac{d\rho_{\rm std}}{da} + 3a^2\left(\frac{1}{2}G_{AB}\dot{X}^A\dot{X}^B - V\right) - a^3\frac{\partial V}{\partial a}. \tag{B.4}$$

Combining terms and dividing by a^2 yields the acceleration equation

$$\frac{\ddot{a}}{a} = -\frac{4\pi G}{3}\left[(\rho_{\rm std} + 3p_{\rm std}) + (\rho_7 + 3p_7)\right], \tag{B.5}$$

with

$$\rho_7 = \frac{1}{2}G_{AB}\dot{X}^A\dot{X}^B + V, \qquad p_7 = \frac{1}{2}G_{AB}\dot{X}^A\dot{X}^B - V. \tag{B.6}$$

B.2 Hamiltonian constraint

The canonical momenta are

$$p_a = -\frac{3}{4\pi G}a\dot{a}, \qquad p_A = a^3 G_{AB}\dot{X}^B. \tag{B.7}$$

The Legendre transform gives

$$H = p_a\dot{a} + p_A\dot{X}^A - L. \tag{B.8}$$

Substituting and simplifying,

$$H = -\frac{4\pi G}{3a}p_a^2 + a^3\rho_{\rm std} + \frac{1}{2a^3}G^{AB}p_A p_B + a^3 V(X;a). \tag{B.9}$$

Time-reparametrization invariance implies the constraint

$$\boxed{H = 0,} \tag{B.10}$$

which leads directly to the Friedmann equation

$$H^2 = \frac{8\pi G}{3}(\rho_{\rm std} + \rho_7). \tag{B.11}$$

B.3 Internal-sector equations of motion

Variation with respect to X^A yields

$$\frac{d}{dt}\left(a^3 G_{AB}\dot{X}^B\right) - a^3\partial_A V + \frac{1}{2}a^3\partial_A G_{BC}\dot{X}^B\dot{X}^C = 0. \tag{B.12}$$

Expanding the time derivative,

$$\ddot{X}^A + 3H\dot{X}^A + \Gamma^A_{BC}\dot{X}^B\dot{X}^C + G^{AB}\partial_B V = 0, \tag{B.13}$$

where

$$\Gamma^A_{BC} = \frac{1}{2}G^{AD}(\partial_B G_{CD} + \partial_C G_{BD} - \partial_D G_{BC}) \tag{B.14}$$

is the Levi–Civita connection on $\mathcal{M}_7$.

B.4 Continuity equation for the internal sector

Multiplying the equation of motion by $G_{AD}\dot{X}^D$ and summing over A gives

$$\frac{d}{dt}\left(\frac{1}{2}G_{AB}\dot{X}^A\dot{X}^B\right) + 3HG_{AB}\dot{X}^A\dot{X}^B + \dot{X}^A\partial_A V = 0. \tag{B.15}$$

Adding $\dot{V}$ and rearranging,

$$\dot{\rho}_7 + 3H(\rho_7 + p_7) = \dot{a}\,\frac{\partial V}{\partial a}. \tag{B.16}$$

In logarithmic form,

$$\boxed{\frac{d\rho_7}{d\ln a} = -3(\rho_7 + p_7) + \frac{\partial V}{\partial \ln a}.} \tag{B.17}$$

B.5 Fixed-point condition

A scaling solution satisfies

$$\frac{d\rho_7}{d\ln a} = 0. \tag{B.18}$$

Using the continuity equation,

$$3(1 + w_7)\rho_7 = \frac{\partial V}{\partial \ln a}. \tag{B.19}$$

This relation defines all cosmological regimes discussed in the main text.

B.6 Entropy flow equation

The entropy functional is

$$\Theta = \log Z, \qquad Z = \int_{\mathcal{M}_7} d\mu_7\, e^{-\beta\mathcal{H}_7}. \tag{B.20}$$

Applying the scale derivative,

$$\frac{d\Theta}{d\ln a} = \frac{1}{Z}\frac{dZ}{d\ln a}. \tag{B.21}$$

Evaluating explicitly,

$$\frac{d\Theta}{d\ln a} = -\left\langle \frac{d\beta}{d\ln a}\mathcal{H}_7 + \beta\frac{\partial\mathcal{H}_7}{\partial\ln a}\right\rangle + \frac{1}{2}\left\langle\frac{d\ln g_7}{d\ln a}\right\rangle. \tag{B.22}$$

This is the entropy flow equation used in Sections 0.5–0.9.

B.7 Linear stability matrix

Linearizing around a fixed point,

$$X^A = X^A_* + \delta X^A, \qquad \Pi_A = \Pi_{A,*} + \delta\Pi_A, \tag{B.23}$$

yields

$$\frac{d}{dN}\begin{pmatrix}\delta X^A \\ \delta\Pi_A\end{pmatrix} = \begin{pmatrix}0 & H^{-1}\delta^A_B \\ -\frac{1}{H}\nabla_B\nabla^A V & -3\delta^A_B\end{pmatrix}\begin{pmatrix}\delta X^B \\ \delta\Pi_B\end{pmatrix}. \tag{B.24}$$

Eigenvalues with negative real parts correspond to stable attractors.

B.8 Summary

All equations employed in the main text follow directly from explicit variation, Legendre transformation, and controlled approximations. No phenomenological equations are assumed. This appendix provides the complete derivational backbone of the L(6+7) framework.

C Numerics, Dataset, and Figures

C.1 Numerical protocol

All numerical results shown in this paper are obtained by integrating the coupled minisuperspace system for the scale factor $a(t)$ and the internal-sector coordinates $X_A(t)$, $A = 1, \dots, 7$, subject to the Hamiltonian constraint and the reduction limits discussed in the main text. We evolve the system in the logarithmic scale variable $N \equiv \ln a$ (so that $d/dt = H\, d/dN$), which provides stable time-stepping across many orders of magnitude in a.

Initial conditions for the internal sector are sampled from a fixed bounded domain in $\mathcal{M}_7$, together with an ensemble over the model parameters (in particular, the two-dimensional scan plane used in the regime maps). Each run is evolved until it reaches a late-time attractor or until a maximal integration time is reached, after which the trajectory is classified by its asymptotic behavior.

C.2 Dataset and derived observables

The core dataset used to construct regime maps consists of an ensemble of $\mathcal{O}(10^5)$ independent runs (approximately 10^5 "universes" in the FRW sense). For each run we record: (i) late-time equation-of-state indicators, (ii) effective energy-density scalings, and (iii) entropy-derived quantities computed from the internal-sector dynamics.

Two summary observables are used throughout the figures:

- The regime entropy statistic $S_{\text{regime}}(\lambda, \alpha)$, which quantifies the coarse-grained organization of trajectories over the internal manifold for fixed model parameters.
- The dark-matter-like fraction $p_{\text{dm}}(\lambda, \alpha)$, defined as the empirical fraction of trajectories whose effective scaling matches the DM-like behavior within the adopted classification thresholds.

The DE-like basin corresponds to trajectories converging to a stable late-time attractor with $w \to -1$, while stiff-like behavior corresponds to kinetic-dominated scaling at late times.

C.3 Figure generation

All phase diagrams and heatmaps are produced by binning the (λ, α) plane and aggregating run-level classifications and entropy statistics within each bin. The figures collected in Appendix D are the minimal set required to reproduce the core claims: (i) the existence of a compact DE basin, (ii) the structured DM-like landscape, and (iii) the correlated transition pattern between stiff/DM/DE fractions.

C.4 Numerics and dataset summary

The dynamical system defined by the constrained Hamiltonian formulation was integrated numerically on a broad parameter grid in the (λ, α) plane. For each sampled point, the evolution was followed across an expanding FRW background, and the late-time behavior was classified into coarse entropic regimes (stiff-dominated, DM-like, DE-like) using stable, code-level criteria (fixed-point convergence, effective equation of state, and regime entropy diagnostics).

The resulting dataset is an ensemble of independent "universe realizations" with per-run metadata (parameter values, final-state observables, and regime labels) suitable for reproducible statistical post-processing. The key empirical outcome is that the DE-like attractor occupies a compact basin in parameter space, while the majority of the domain is stiff-dominated; an intermediate DM-like sector appears as a structured region correlated with the entropy landscape.

C.5 Figures used in this version

For the v1 release we restrict attention to a minimal, publication-grade figure set: (i) a global phase diagram of regimes, (ii) a zoom on the compact DE basin, (iii) a map of the DM-like fraction, (iv) an entropy map characterizing the internal-sector organization, (v) a representative transition pattern stiff→DM→DE, and (vi) an overall meta-entropy landscape summarizing regime structure. These figures are collected in Appendix D and are generated directly from the ensemble statistics, ensuring a clean trace from numerical output to plotted results.

D Figures

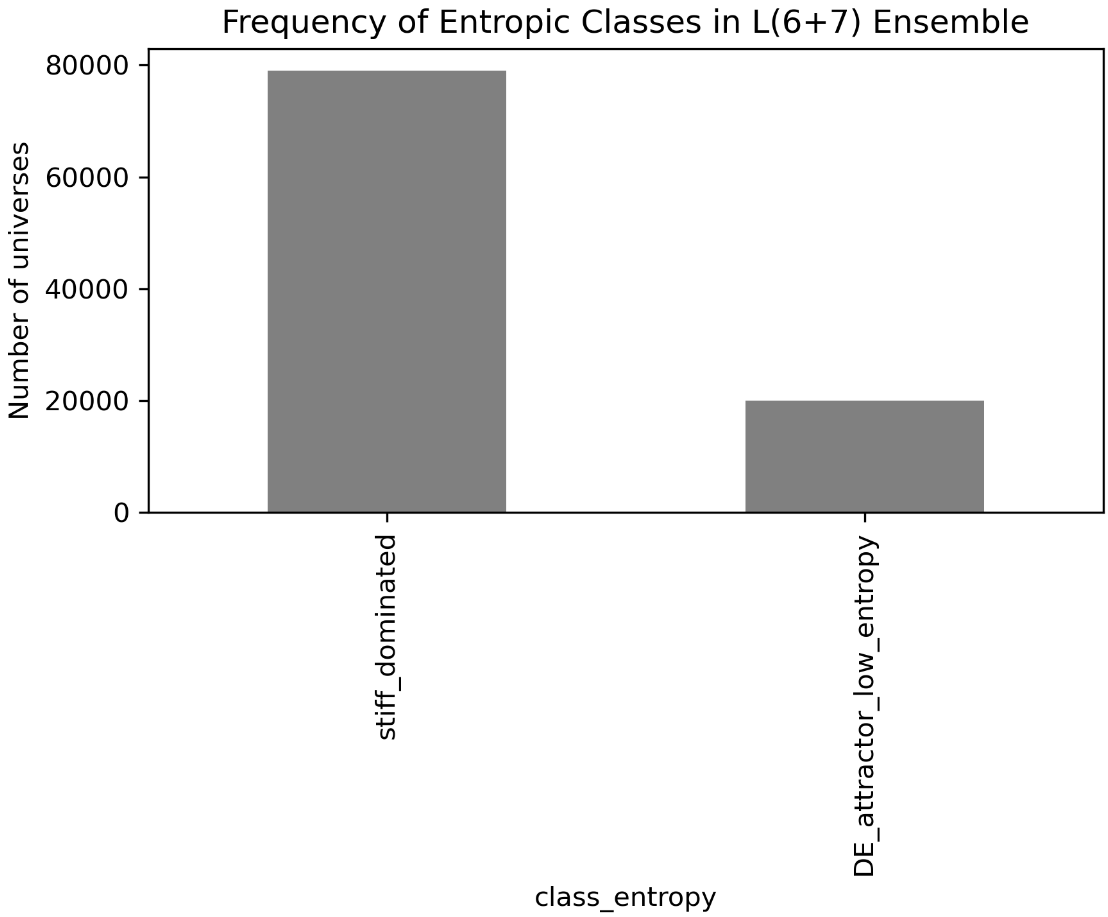

Figure 1: Frequency of entropic classes in the L(6+7) ensemble. The stiff-dominated sector occupies the majority of the sampled parameter space, while a smaller subset converges to a low-entropy dark-energy attractor.

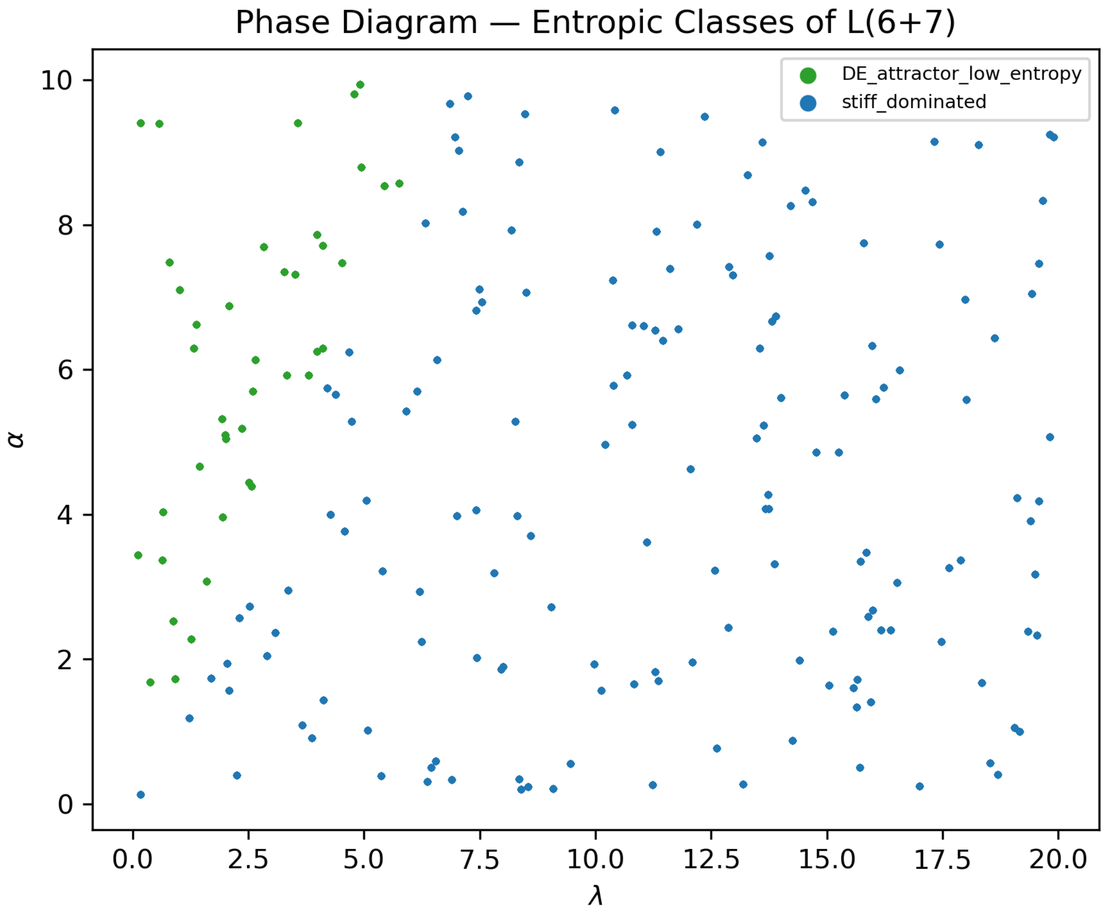

Figure 2: Phase diagram of entropic classes in the (λ, α) plane. The dark-energy attractor forms a compact basin, while the remainder of the plane is predominantly stiff-dominated.

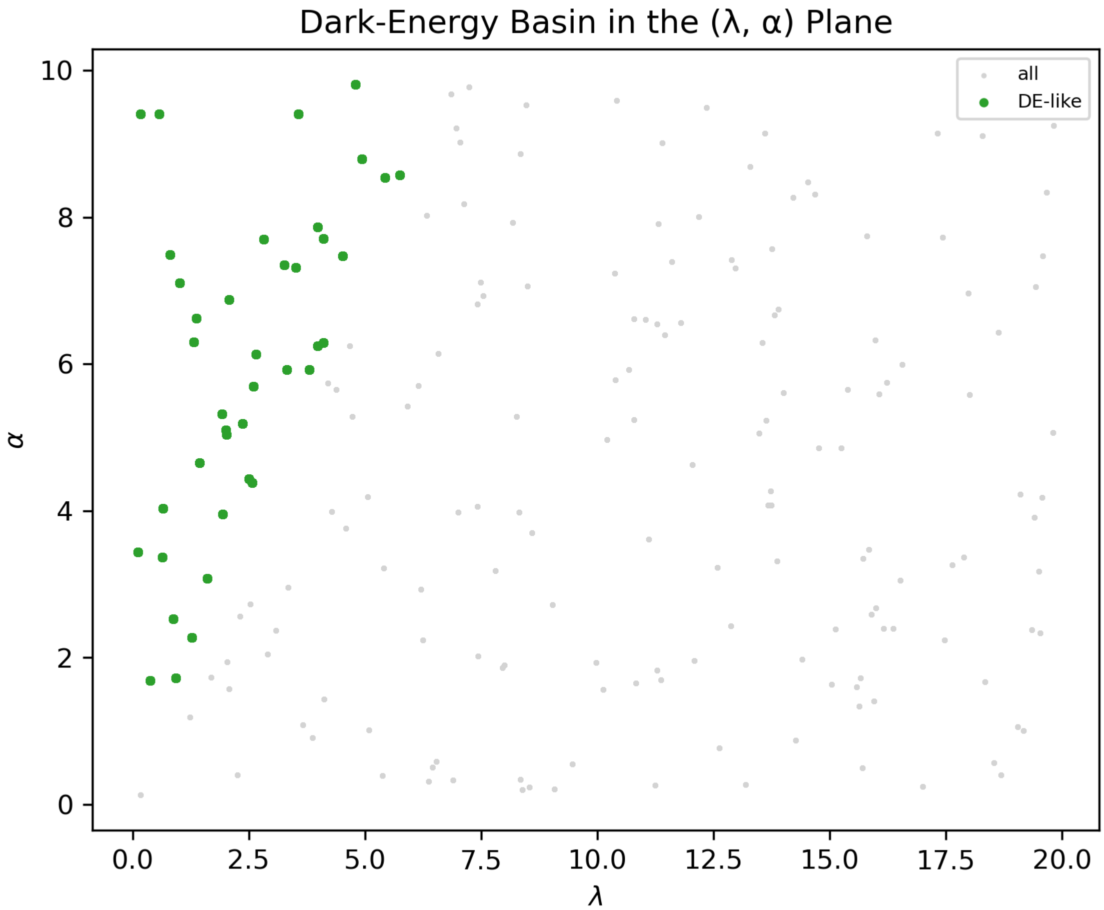

Figure 3: Zoom on the compact dark-energy basin in the (λ, α) plane. Points classified as DE-like cluster into a sharply localized region, supporting a structured regime landscape rather than a diffuse fine-tuning band.

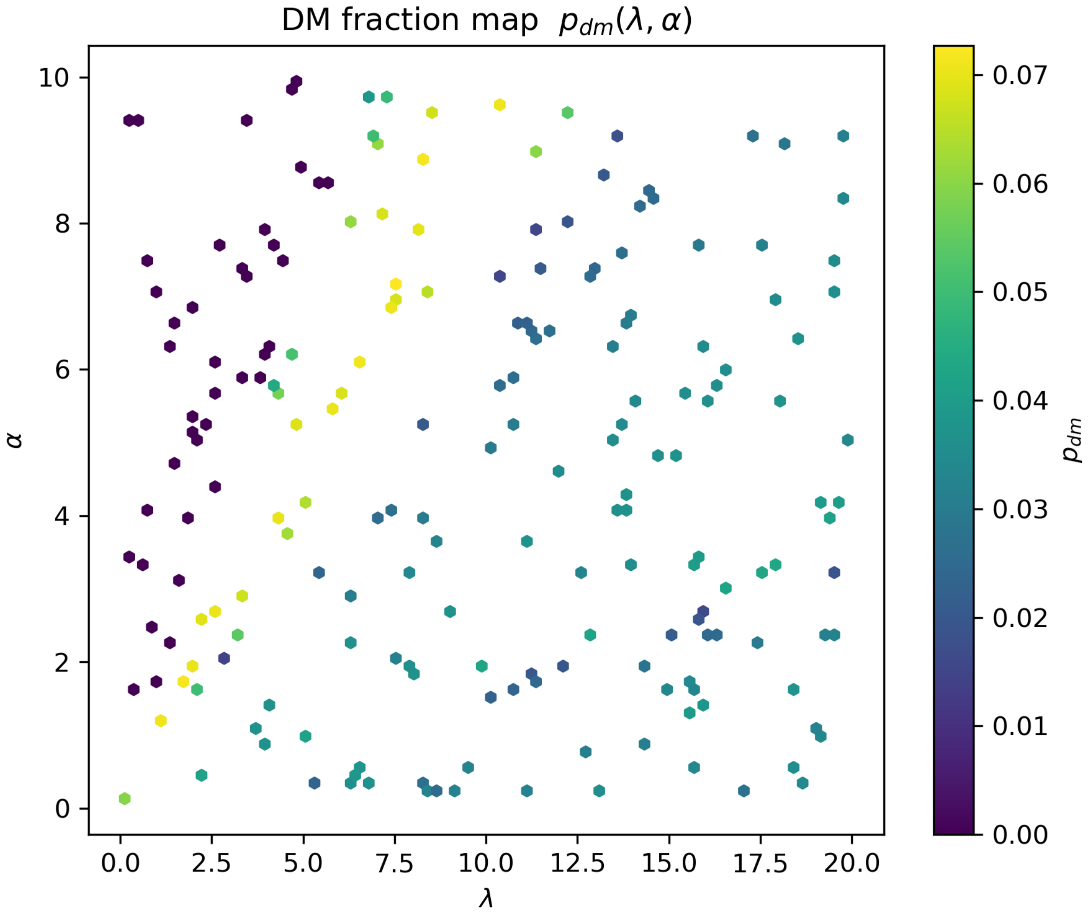

Figure 4: Map of the dark-matter-like fraction $p_{\mathrm{dm}}(\lambda, \alpha)$ across the sampled parameter space.

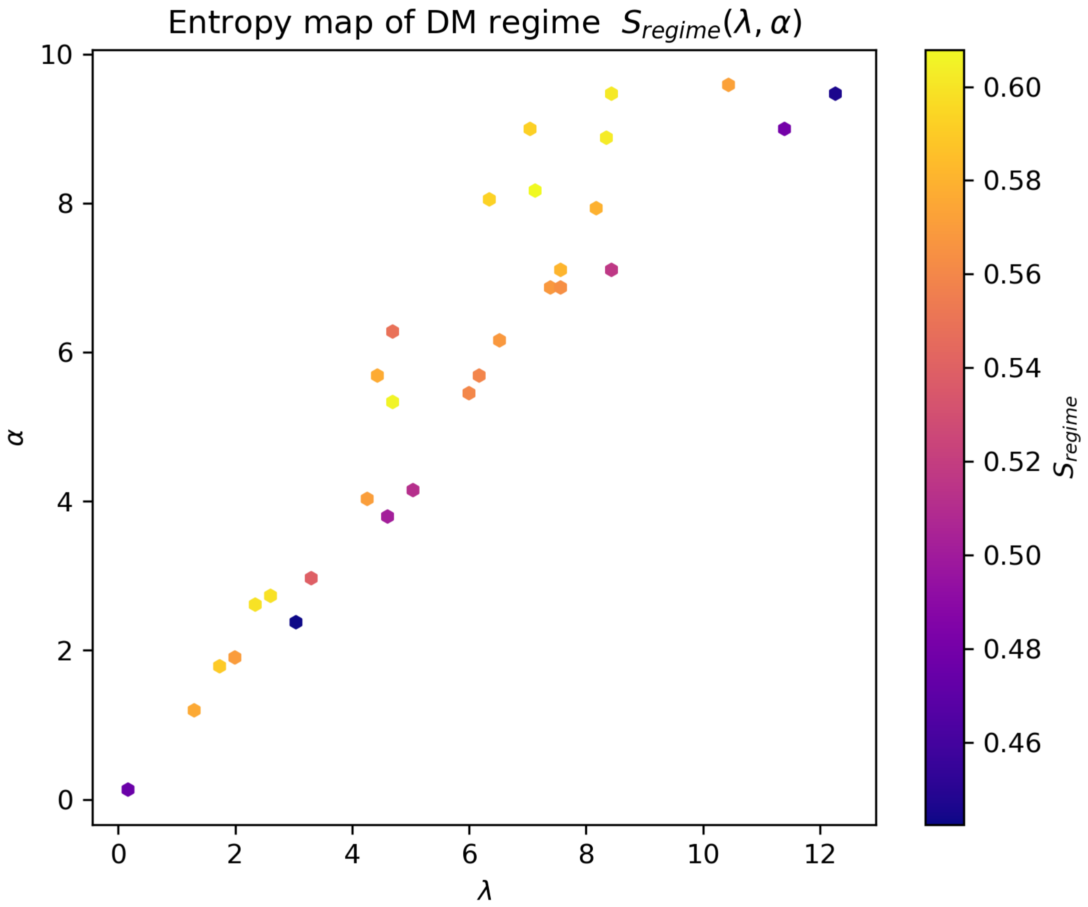

Figure 5: Entropy map $S_{\text{regime}}(\lambda, \alpha)$ for the DM-like regime. The structure correlates with the DM fraction landscape and highlights organized statistical behavior in the internal sector.

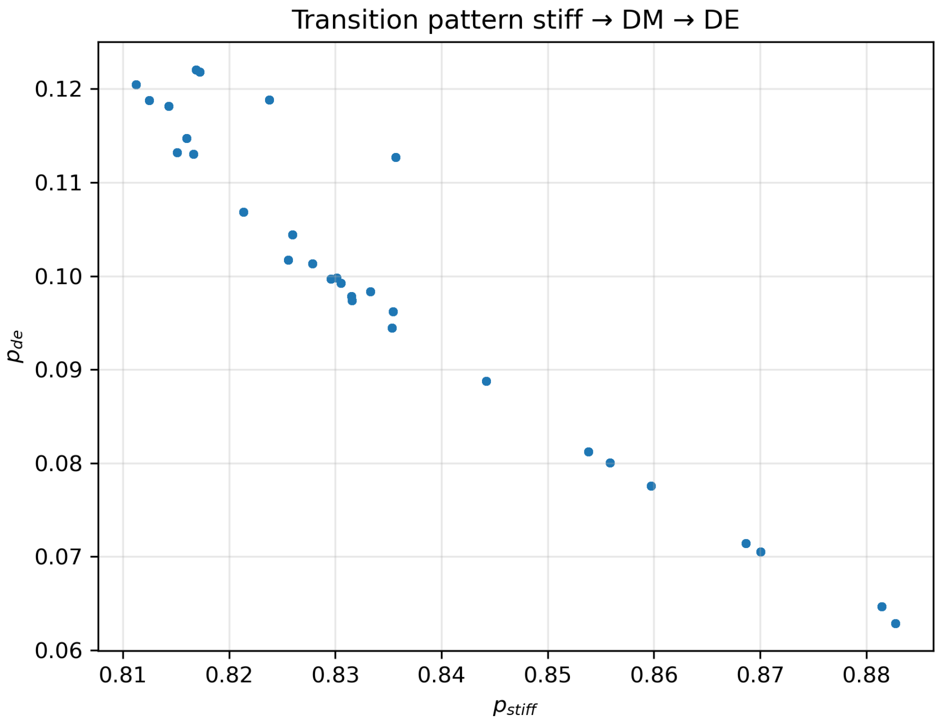

Figure 6: Transition pattern stiff $\rightarrow$ DM $\rightarrow$ DE observed in the ensemble statistics, shown as a correlated trend between regime fractions.

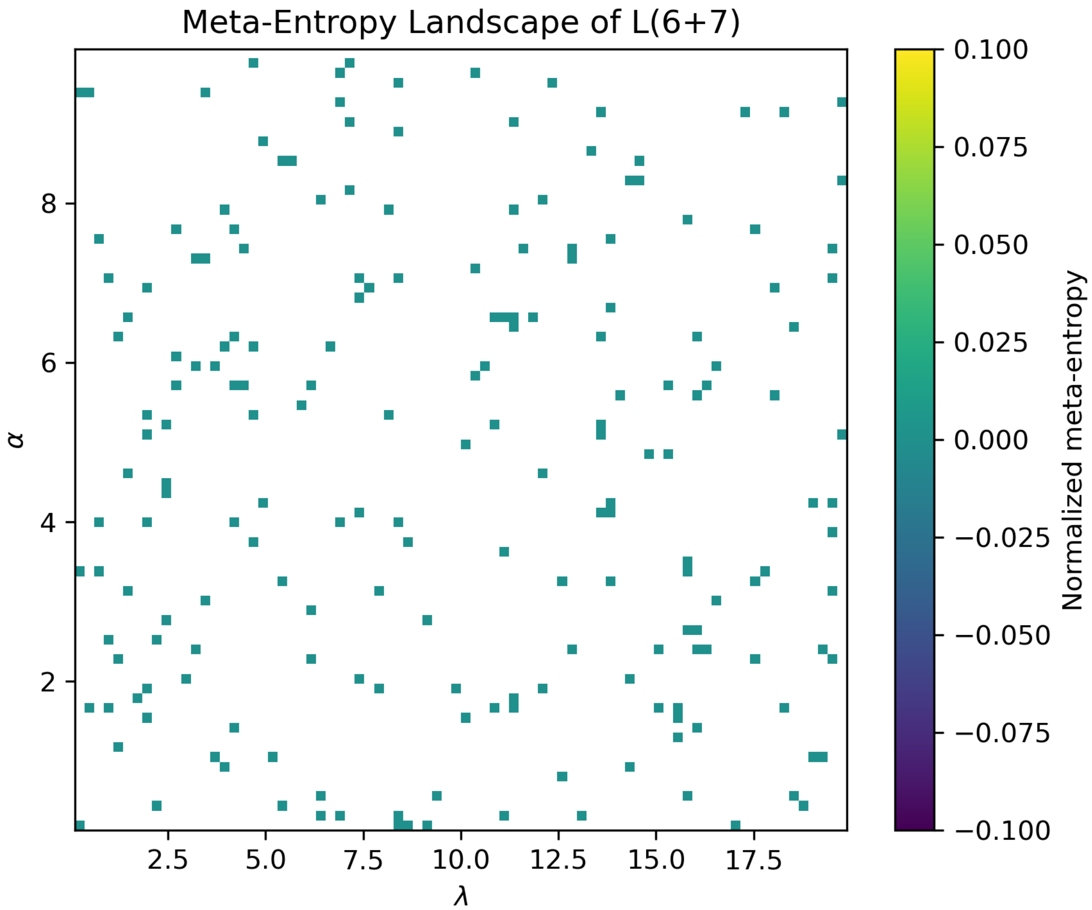

Figure 7: Meta-entropy landscape in the (λ, α) plane. This summarizes the structured organization of regimes induced by the internal (+7) sector.